aerospace

MDPI

Review

A Survey of Precision Formation Relative State Measurement Technology for Distributed Spacecraft

Zhang Zhang [1,2,3,*], Lei Deng [1,3], Jiaqi Feng [1,2], Liang Chang [1,3], Dong Li [1,3] and Yilin Qin [1,2]

[1] Innovation Academy for Microsatellites of Chinese Academy of Sciences, Shanghai 201203, China; deng_leo@163.com (L.D.); fengjq@microsate.com (J.F.); changl@microsate.com (L.C.); lid@microsate.com (D.L.); qinyilin20@mails.ucas.ac.cn (Y.Q.)
[2] University of Chinese Academy of Sciences, Beijing 100039, China
[3] Shanghai Engineering Center for Microsatellites, Shanghai 201203, China
* Correspondence: zhangz@microsate.com

Abstract: High-precision relative-state measurement technology is one of the key technologies for achieving the precision formation flying of distributed spacecraft. This paper conducts a comprehensive analysis of the precision formation-flying projects of distributed spacecraft in various countries. In the context of practical application, the specific mission configuration, orbit distribution, measurement technology, and payload of the project are summarized. On this basis, the relative state measurement techniques are outlined for the first time, using non-autonomous measurement techniques, autonomous measurement techniques, and new composite relative measurement techniques. A detailed analysis of GNSS (Global Navigation Satellite System)—relative measurement, laser measurement, infrared measurement, RF measurement, visible light visual measurement, and multiple composite measurement methods is conducted. The applicable scenarios of each measurement method are thoroughly discussed from several aspects, such as the technical scheme, system design, accuracy requirements, advantages, and shortcomings. In addition, this paper proposes the concept of adopting a multidisciplinary optimization architecture from the perspective of the overall design of the precision formation of the distributed spacecraft. It enables relative-state measurement payload selection and property indicator optimization, on the premise of optimizing the overall formation performance. Finally, the optimization direction and future development trend of the spacecraft precision formation flight project and relative state measurement technology are established.

Keywords: distributed spacecraft; precision formation flying; relative state measurement; multidisciplinary optimization

Citation: Zhang, Z.; Deng, L.; Feng, J.; Chang, L.; Li, D.; Qin, Y. A Survey of Precision Formation Relative State Measurement Technology for Distributed Spacecraft. *Aerospace* **2022**, *9*, 362. https://doi.org/10.3390/aerospace9070362

Academic Editor: Mikhail Ovchinnikov

Received: 17 May 2022
Accepted: 2 July 2022
Published: 6 July 2022

1. Introduction

With the continuous exploration of space, spacecraft formation flying has become a hot topic in the aerospace field [1]. The spacecraft formation utilizes a variety of sensors to form a "large virtual spacecraft" to complete high-precision and high-complexity space missions that cannot be completed independently by a single spacecraft [2]. While saving costs, it improves sensitivity and reliability, greatly optimizes the overall performance of the spacecraft system and expands the application field.

Depending on the closeness of the dynamics between the formation spacecraft, as shown in Table 1, formation flying can be divided into precision formation, cooperative formation, and knowledge formation. Precision formations apply relative measurement and precision control techniques to maintain the formation shape and position for long periods of time, with specific applications that include virtual telescopes and synthetic aperture radars. Due to the increasing difficulty of space tasks, precise spacecraft relative measurement technology, as the cornerstone of formation control and the key to autonomous relative navigation, faces many challenges. In view of this key technology, this paper outlines the current research status of distributed spacecraft precision formation

projects and analyzes the technical characteristics and application scenarios of relative state measurement technology, such as GNSS, radio, laser, vision, and new composite technologies. The optimization method and development trend of the relevant technologies are further elaborated.

Table 1. Example of spacecraft formation flying.

Formation Flying Type	Mission	Technical Features	Control Precision
Precision Formation	Three-dimensional stereo imaging, virtual telescope, synthetic aperture radar, synthetic aperture optical interferometry, gravitational wave detection	Through autonomous navigation and precision control technology, precise shapes and poses can be maintained between spacecraft over time	Long-term continuous precision measurement control
Knowledge Formation	Ground-probing, Intermittent three-dimensional passive navigation	Mutual measurements exist between the spacecraft, but coupling control is not required	Independent control
Collaborative Formation	Rendezvous docking, twin formation flight and fly-around	Spacecraft maintain relative measurement and control for short periods of time during the mission	Precision measurement control stages

2. Research Status of the Precision Formation of Distributed Spacecraft Project

2.1. TechSat-21

TechSat-21 (Technology Satellite of the 21st Century) [3] is a program that was developed by the US Air Force Research Laboratory in 1998 to validate synthetic radar technology. The project consists of an 8–16 formation of small satellites to form a large virtual satellite; the satellites are distributed in a polar orbit of 800 km. The virtual satellite uses electromagnetic wave interference to complete relative state measurements and meet the requirements of rapid mission-formation shape transformation. The GPS relative measurement payload weighs 4 kg, with a power consumption of about 50 W. Figure 1 shows the schematic diagram of the virtual satellite's sparse aperture, which is a distributed SAR system with multiple transmissions and multiple receivers that is mainly used for ground motion indication and ground elevation measurement. The relative position accuracy is required to be 1–10 cm in order to maintain the formation's large and effective radar aperture [4].

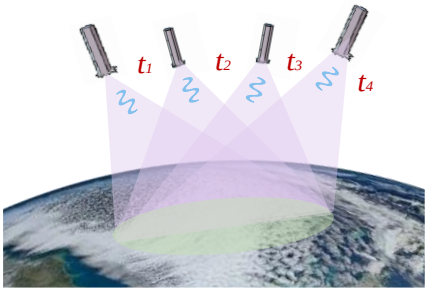

Figure 1. Diagram of the sparse aperture observation.

The project achieved remarkable results in the early stages. Due to the level of technology, as well as cost constraints, the project was forced to end in 2003, but it has demonstrated a new breakthrough in spacecraft formation flight technology.

2.2. Darwin

The Infrared Space Interferometer program [5], known as Darwin, was proposed and implemented by the European Space Agency (ESA) in 1993. It is composed of 4–9 spacecraft.

The mission is to search for Earth-like planets among the stellar planets, determine the composition of planetary atmospheres, and infer the possibility of signs of life from them. Darwin can achieve high spatial resolution in the infrared wavelength region and is the first program to search for an exoplanet. The optimal formation of spacecraft was determined as follows: four spacecraft (the collecting spacecraft, CS) are configured with 3–4-meter astronomical telescopes forming a quadrilateral (the Darwin Emma X-array), and one spacecraft (the beam-combiner spacecraft, BCS) focusing the beam, as shown in Figure 2. In order to meet the requirements of interferometry, the formation is located at the L2 point where the spacecraft hovers under force balance; it is necessary to maintain high-precision control during maneuvering. The project was canceled in June 2011 for technical and budgetary reasons.

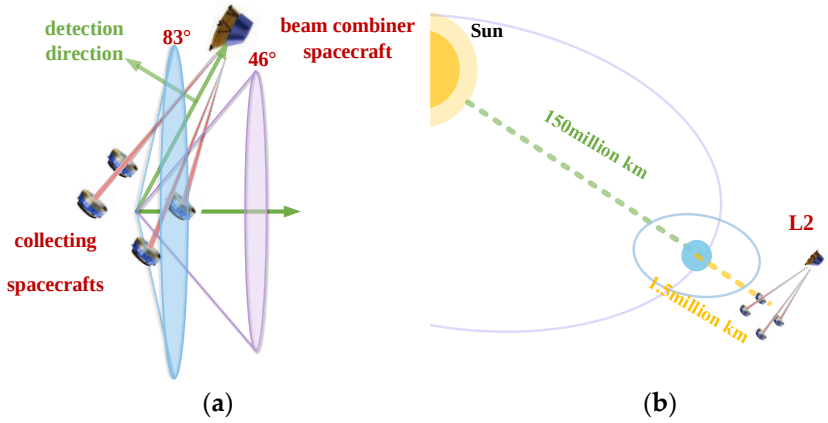

Figure 2. Diagram of the Darwin project. (**a**) Formation shape of Darwin, (**b**) Space orbit schematic of Darwin.

2.3. PRISMA

PRISMA (Prototype Research Instruments and Space Mission Technology Advancement) [6] was launched on 15 June 2010 and was funded by the Swedish National Space Board. It consisted of two microsatellites, Mango (95 kg) and Tango (50 kg). The mission was to verify the M-level autonomous formation, approach, and rendezvous stop technology, and to perform precise control at DM-level in a sun-synchronous orbit at an orbital altitude of about 700 km. GNSS signals are unreliable in this case, due to the altitude of the formation flight orbit. The spacecraft adopted the formation flight RF system, developed by CNES (French Space Agency), to provide stable autonomous measurements during the mission, as shown in Figure 3, to realize formation-flying technology verification and ground detection [7].

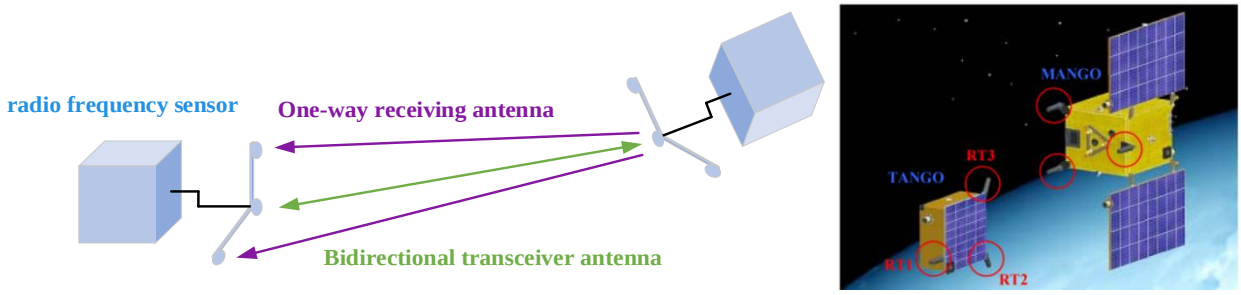

Figure 3. The relative-state measurement FFRF system; the antenna structure of PRISMA.

For the first time, the project carried out a dual-orbit spaceborne autonomous formation flying experiment (SAFE) in low-Earth orbit and achieved an innovative relative navigation technology verification of GPS with a vision-based sensor (VBS) and formation flying radio frequency (FFRF). SAFE is divided into four stages, as shown in the Table 2. The

project used a GPS, FFRF (formation flying radio frequency) sensor, and VBS (vision-based sensor) to measure the distance between satellites. The rough stage distance measurement accuracy was 10 cm, and the effective distance was 30 km; the precision stage distance measurement accuracy was 1 cm, and the effective distance was 250 m.

Table 2. SAFE verification phases.

Validation Phase	Measurement Technology	Measurement Range
Autonomous Formation Flying	Phoenix-S GPS Receiver System Formation Flying Radio Frequency (FFRF)	20 m~10 km
Homing and Rendezvous	Vision-Based Sensor (VBS)	3 m~100 km
Precision Three-dimensional Proximity Operations	Phoenix-S GPS Receiver System Vision-Based Sensor (VBS)	3~100 m
Final Approach and Recede Maneuvers	Vision-Based Sensor (VBS)	0~3 m

2.4. XEUS

XEUS (X-ray Evolving Universe Spectroscopy) is a potential successor mission to XMM (X-ray Multi-mirror Mission), proposed by the ESA in 1996 [8]. It was incorporated into the International X-ray Observatory (IXO) project in 2008, followed by the Advanced Telescope for High-energy Astrophysics (ATHENA) for study in 2011. XEUS comprises a main detector (DSC) and a mirror spacecraft (MSC) 50 m apart to form an X-ray virtual telescope in orbit L2. The relative position measurement is carried out by the laser, as shown in Figure 4. The mission-design life of XEUS is greater than 25 years. The distance measurement accuracy is on a sub-micron scale, with an effective range of 40 cm $\pm$ 1 m, and the surface offset measurement accuracy is 125 microns, with an effective range of $\pm$1 m; the roll angle measurement accuracy is 8 seconds, and the pitch and yaw angle accuracy are up to 1 seconds. The laser probe of the DSC is controlled by the system, which can measure the relative pose of the target spacecraft [9].

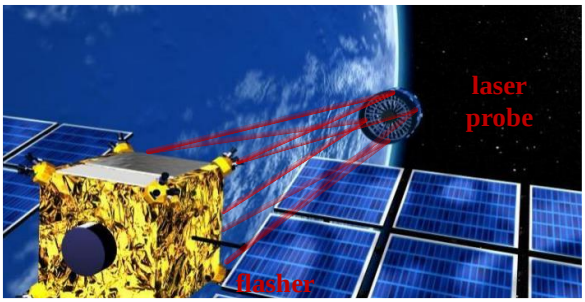

Figure 4. Diagram of the virtual telescope, XEUS.

2.5. LISA

LISA (Laser Interferometer Space Antenna) [10] was a gravitational wave observatory jointly established by NASA and the ESA. It was introduced in 1998. In 2011, NASA withdrew from the development due to funding reasons. The ESA simplified the mission configuration side length from 5 million km to 1 million km and renamed it the eLISA program. The goal of this project is to detect gravitational waves, with a focus on detecting the mergers between deep blank dwarf binaries and black holes. LISA is composed of three spacecraft with a height of 1.8 m, equipped with laser interferometers to form a triangle. They are positioned in a heliocentric orbit, following the Earth around the sun to detect the characteristics of gravitational waves, as shown in Figure 5, with a measurement accuracy of 1 μm. The three spacecraft independently conduct relative state measurements and formation maintenance. The current plan establishes a side length of 2.5 million km, with a measurement accuracy of 10 m [11].

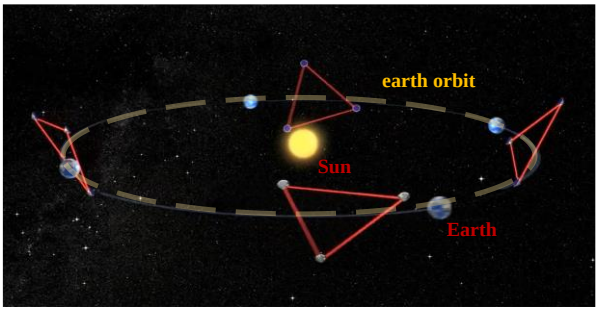

Figure 5. Space orbit schematic of LISA.

2.6. GRACE and GRACE Follow-On

The Gravity Recovery and Climate Experiment (GRACE) [12] was launched by NASA in 2002. The project consisted of two spacecraft with orbits of 500 km and a separation of 100–150 km. The task was to measure the gravitational potential coefficient through relative distance changes in the co-orbiting spacecraft and to conduct observational research on the Earth's water quality [13], geology, and climate. The inter-satellite status is measured using a two-way K-band ranging system (KBR), with the payloads shown in Table 3. GRACE-2 satellite was retired in 2017 due to battery aging. In May 2018, NASA and the German Earth Science Research Center jointly launched GRACE Follow-On (GRACE-FO) to continue the mission. In addition to the Super STAR accelerometer, KBR system, star sensor, laser-ranging angular reflector, and BLACKJACK dual-band GPS receiver [14], a new laser rangefinder was introduced to improve accuracy.

Table 3. Payloads performance of GRACE.

Payloads	Measurement Accuracy	Function
K-band ranging system (KBR)	1 μm/s	Measuring changes in the Earth's gravity field
Super STAR accelerometer	1 nm/s^2	Measuring non-gravity-induced acceleration
Star sensor	0.1 mrad	Spacecraft altitude measurement
BLACKJACK GPS receiver	1 mm	Spacecraft relative state determination
Laser backward reflector	1 mm	Auxiliary GPS for precision orbiting

2.7. CanX-4/CanX-5

CanX-4/CanX-5 [15] is a Canadian Space Agency-funded formation project developed by the University of Toronto, Canada, comprising two spacecraft in formation at a distance of 500–1000 m, as shown in Figure 6. Its mission is the verification of the autonomous formation flight technology in sub-meter-precision spacecraft. CanX-4 and CanX-5 are identical cubic micro–nanosatellites with a mass of 7 kg. The satellite altitude system consists of a three-axis magnetometer, three rate gyros, six sun-sensors, and three orthogonally mounted reaction wheels. The satellites are equipped with four 5-mN cold gas thrusters (sulfur hexafluoride) oriented in a single direction for orbital maneuvers. The formation satellites are configured with GPS receivers to transmit status information and use the S-band inter-satellite link to transmit status information, with a measurement accuracy of 10 cm.

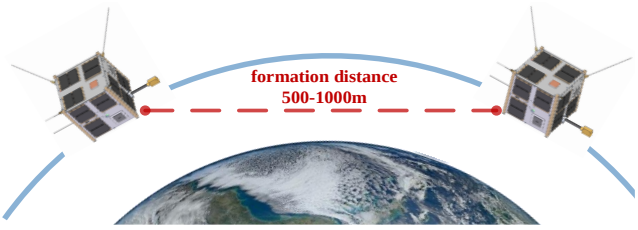

Figure 6. Schematic diagram of the CanX-4/CanX-5 formation flight.

2.8. Proba-3

The Proba-3 [16] program, proposed by the ESA and scheduled for launch in 2023, consists of a tracking satellite (200 kg Occulter dwarf satellite) and target satellite (340 kg Coronagraph satellite). The purpose of the mission is to demonstrate techniques for high-precision spacecraft formation flying. Coronagraph's and Occulter's GNC system comprises four reaction wheels, three three-axis gyros, a three-headed star tracker, six solar sensors, and two GPS receivers [17].

The Proba-3's first task will be to verify the GPS and radio data to perform relative position measurement, including both rough measurement and precise measurement. The second task is to create a 100–150 m satellite formation at the apogee to survey the artificial solar eclipse. The relative state measurement used by Proba-3 includes the relative tangential coarse measurement between satellites (coarse lateral sensor, CLS), GPS longitudinal relative position measurement, and longitudinal fine measurement (Fine Lateral and Longitudinal Sensor, FLLS), as shown in Table 4. The formation distance between satellites ranges from 25 m to 250 m, and the formation is only maintained at the apogee. According to the accuracy requirements of the task, RF (radio frequency) sensors, GPS, and optical measurement systems will be used to achieve state measurement.

Table 4. Proba-3 measuring system performance indicators.

Methods	Item	Effective Range	Measurement Accuracy
GPS	Z distance	Perigee Apogee	7.5 cm 10 cm
CLS	X-Y plane offset	150 m	1 mm
FLLS	Z distance X-Y plane offset	25–250 m 20.5 mm	30 µm 21 µm

2.9. TerraSAR-X, TanDEM-X

TanDEM-X [18], a radar satellite jointly developed by EADS (European Aeronautic Defence and Space company) Astrium and the German Aerospace Center (DLR), was launched on 15 June 2007. On the basis of its high-resolution mission, a radar satellite called TerraSAR-X was added to form a dual-satellite high-precision synthetic aperture radar interferometer, which was completed on 21 June 2010 [19]. This project adopted a dual-frequency GPS receiver ranging system to achieve the high-precision measurement of inter-satellite baselines. Similar to the GRACE system, the spiral formation shape was used to achieve complete synthetic aperture imaging. The space baseline estimation accuracy needs to reach 1 mm to complete this precision Earth observation mission. The orbital altitude of the satellite is 514 km, and the satellite utilizes an active X-band phased array SAR antenna, a laser angle reflector, a ranging TOR (a tracking, occultation and ranging device), and a dual-frequency GPS occultation receiver (GPS occultation receiver and IGOR). IGOR's carrier phase accuracy reaches the mm level. The formation can complete flexible interference modes, including dual-station chase, single-station chase, and switching chase modes.

2.10. Gemini

The Gemini (GPS-based Orbit Estimation and Laser Metrology for Intersatellite Navigation) project was initiated by the German Space Operations Processing Center [20] in 2001. Gemini is composed of two satellites with a mass of approximately 80–100 kg and an orbital plane altitude of 500–700 km. The state measurement payloads on each satellite include GPS receivers, pulsed LiDARs, and laser interferometers. The payload weighs 30 kg, and the power is about 70 W. Gemini's first mission was the verification of key technologies of formation flying, including laser measurement tracking technology, autonomous orbit control technology, and a closed-loop formation control strategy; mission two was high-resolution Earth-observation imaging. To accumulate experience to aid in

the upcoming formation-flying mission, the formation shape would constantly be changed, as shown in Figure 7 and Table 5.

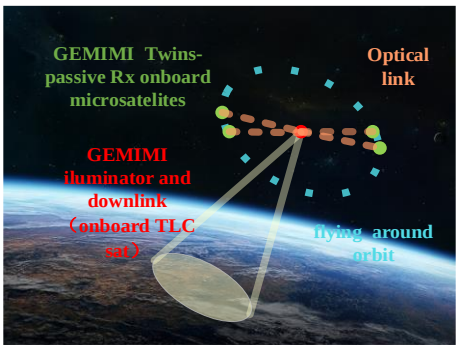

Figure 7. Schematic diagram of the Gemini project.

Table 5. Gemini accuracy indicators.

Formation Distance	Measurement Accuracy	Control Accuracy
>100 km	m	10 m
>1 km	cm–dm	m
<1 km	mm	cm

2.11. CANYVAL-X

CANYVAL-X [21] is a cooperation project between Yonsei University, the Korean Institute of Aeronautics and Astronautics, and NASA and was launched in December 2018. It consists of two cube satellites, named Tom and Jerry. One of the two satellites is used as the lens system, and the other is used as the detector system, forming a virtual telescope system, as shown in Figure 8. The mission is to verify the inertial alignment system of the target (the sun). The project utilizes a tandem telescope during the flight and observes celestial objects near the bright radiation source by blocking the radiation of the target celestial object in the line-of-sight direction of the other satellite. The relative-state measurement method of the program is based on vision measurement technology using visible light. The main satellite is fitted with a visual camera, while the slave satellite is equipped with a laser diode. The measurement of the relative state between the satellites is completed using image projection. The altitude measurement control accuracy is 1°, the position measurement accuracy is at an approximately dm level, and the control accuracy is at approximately m level. The relative measurement accuracy is shown in the figure.

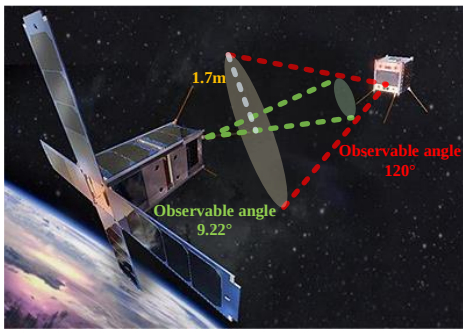

Figure 8. Schematic diagram of CANYVAL-X.

2.12. TianQin

The Tianqin project, jointly developed by Sun Yat-sen University and the Huazhong University of Science and Technology, was proposed by Luo Jun, an academician of the

Chinese Academy of Sciences, in 2016 [22]. The system was made up of three spacecraft in a geocentric orbit, forming an equilateral triangular configuration with a side length of 170,000 km, as shown in Figure 9. The orbital altitude of the project was approximately 100,000 km. Tianqin, a large space gravitational wave detector, has a telescope diameter of 0.2 m and uses the binary white dwarf J0806 as the detection source. The purpose of the mission is to use the detection of gravitational waves to complete the study of astrophysical processes, realize the precise test of general relativity, and further study the origin of and changes to the universe. The principle of gravitational wave detection and the required core technologies include responsive inter-satellite laser interferometry technology and space inertial reference technology. At present, the program has completed its first launch; Tianqin-1 was launched on 20 December 2019 [23].

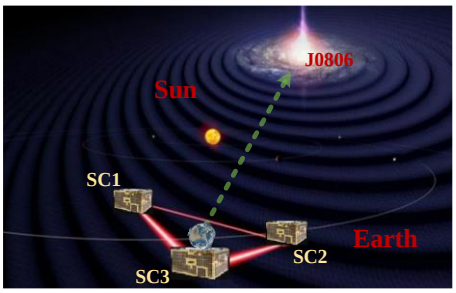

Figure 9. Schematic diagram of TianQin.

2.13. TaiJi

The TaiJi project was proposed and developed by the Chinese Academy of Sciences in 2016. As shown in Figure 10, similar to the LISA scenario, TaiJi also forms an equilateral triangle formation on a heliocentric orbit, deviating from the Earth–sun direction by 18–20°. The distance between the spacecraft is 3 million km, and the orbit height is approximately 50 million km [24]. The project completed the 0.1 mHz–1 Hz mid- and low-frequency gravitational wave detection plan by establishing a laser link. The difference is that the TaiJi program formation configuration has a side length of 3 million km. It is more technically difficult to maintain the necessary coordinated ultra-stable and ultra-quiet platform of the spacecraft formation. The laser interferometric system consists of a highly stable laser light source, a highly stable laser telescope, a laser interferometer, a phase meter, an ultra-stable clock, a laser capture system, and a noise suppression system. The program was divided into three phases, first launching the Taiji-1 satellite, further completing the double-satellite formation, and finally completing the triple-satellite formation. Taiji-1 was launched on 31 August 2019 and completed the in-orbit test [25].

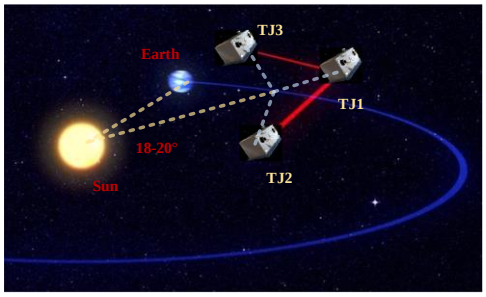

Figure 10. Schematic diagram of TaiJi.

2.14. IRASSI

InfraRed Astronomy Satellite Swarm Interferometry (IRASSI) [26] was proposed by the German Aerospace Center's Space Administration (DLR) in 2016. It consists of five spacecraft, forming a 3.5 m infrared interferometer with orbits distributed at point L2 and

an effective detection range of 1–6 Hz, as shown in Figure 11. This project uses far-infrared heterodyne interferometry to study the physical formation process of terrestrial planets, mainly in the cold regions of the universe, stellar disks, etc. The formation range of the telescope satellites is 7–850 m, the baseline measurement accuracy must be less than 5 μm, and the pointing accuracy of the telescope needs to be less than 0.4 arcsec to complete high-precision detection. Each spacecraft is 5.5 m high, equipped with a 6-meter-diameter shading plate and a ranging system composed of four laser modules, forming a three-dimensional asymmetric double-cone telescope array. A detection mission is performed through free drift expansion and the controlled contraction of the formation shape, with a free drift period of 26 h and a controlled contraction period of 22 h [27].

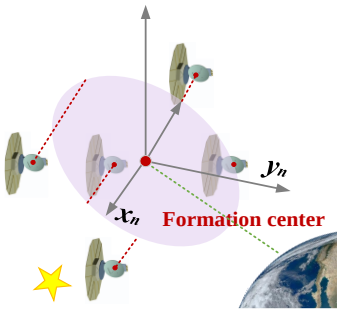

Figure 11. Schematic diagram of IRASSI.

2.15. Trend Analysis of the Distributed Precise Spacecraft Formation Flying Project

With the continuous development of space exploration missions, distributed spacecraft precision formation flying has become a research hotspot in the field of aerospace, and its related technologies have also achieved remarkable progress. It has promoted in-depth engineering practice and theoretical research in numerous international universities and institutions.

As shown in Figure 12 and Table 6 below, the international precision spacecraft formation-flying program began to develop in 1993 and reached its peak period of development in 2005. The task requirements can be roughly divided into three stages. Phase 1 is the technical verification of a low-Earth-orbit precision spacecraft formation flying project, RF precision relative measurement technology verification, visual precision relative measurement technology verification, space laser precision relative navigation technology verification, etc. Phase 2 is the formation of large virtual satellites, such as SAR, hard X-ray modulation telescopes, and infrared interferometers, to complete Earth, sun, and other observation tasks. Phase 3 is progress toward the development of scientific research, such as space gravitational wave detection, which requires higher precision, whereas deep space exploration needs greater autonomy. The mission orbit also begins to develop from a low-Earth orbit to a high orbit, L2 point, and deep space. This type of development is indistinguishable from the progress of relative measurement technology. It also reveals the development direction of technology, which will be explained below.

The accuracy of relative state measurement is indivisible from the formation configuration. Different baseline length ranges will produce results with different accuracies. Moreover, due to different technical characteristics, relative state measurement methods have different valid ranges and applicable scenarios, as shown in Figure 13. Mission requirements determine the configuration, orbit, and accuracy, which, in turn, define the appropriate relative navigation method. As shown in Figure 14 below, from the *y*-axis to the *x*-axis, the accuracy required by the mission is constantly improving: precision formation flying technology verification, space synthetic aperture radar, an infrared interferometer, and laser gravitational wave detection. For example, transferring from CanX-4, with a baseline of 500 m and cm-level accuracy, to LISA and other future formations with a baseline of a million kilometer-level and pm-level accuracy is a very major leap for laser-based relative measurement technology. The specific accuracy is as follows.

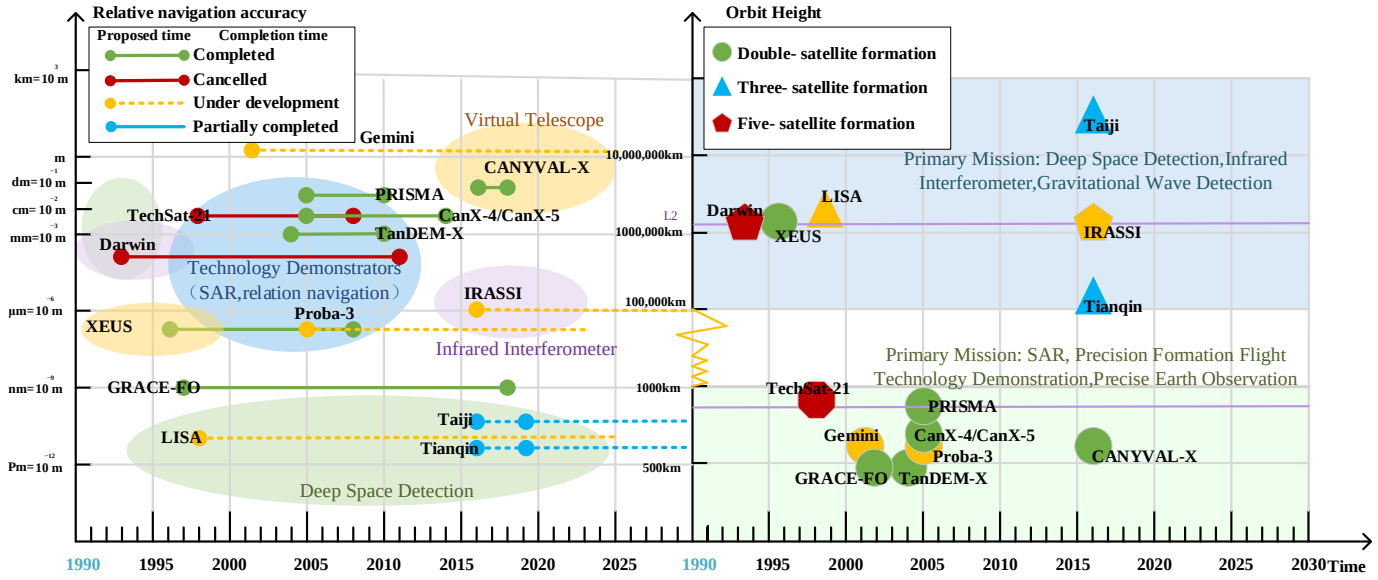

Figure 12. Time analysis chart of the distributed spacecraft precision formation flying projects.

Table 6. The precise formation parameters of each project.

Project	Country/ Institution	Methods	Modes	Measurement Items	Precision	Number	Whether Launch
Techsat-21	USA	GPS	—	Inter-satellite baseline measurements	1–10 cm	8–16	Canceled
TerraSAR-X TanDEM-X	Germany	Laser GPS	—	Inter-satellite baseline measurements	2–4 mm	2	Launched June 2010
PRISMA	Sweden	RF GPS	Rough mode	Z-direction distance (≤30 km) X-Y angle measurement (360°)	10 cm | 5°	2	Launched June 2010
			Precision mode	Z-direction distance (≤250 m) X-Y angle measurement (10 × 10°)	1 cm | 0.2°		
CanX-4/5	Canada	GPS	—	Inter-satellite baseline measurements	Submeter-level	2	Launched June 2014
GRACE-FO	USA(NASA)	RF GPS Laser	—	Inter-satellite baseline measurements	100–10 nm	2	Launched May 2018
CANYVAL-X	Korea	Visible light GPS	—	Direction distance X-Y angle measurement	Approximate dm level | 1°	2	Launched December 2018
TianQin	China	Laser Interference	—	Interferometric ranging	1 pm/ $\sqrt{}$Hz	3	Partial launched

Table 6. *Cont.*

Project	Country/ Institution	Methods	Modes	Measurement Items	Precision	Number	Whether Launch
TaiJi	China	Laser Interference	—	Interferometric ranging	100 pm	3	Partial launched
XEUS	ESA	Laser GPS	—	Z-direction distance (40 cm + 1 m) X-Y surface offset (0 m + 1 m) Roll, pitch and yaw angle	10 μm | 125 μm 8″ | 1″	2	No launch
Gemini	Germany	Laser GPS	Rough mode	Z-direction distance (>100 km)	m-level	1 + 2 × n	No launch
			Precision mode	Z-direction distance (>1 km)	cm-dm level		
			Ultra-precision mode	Z-direction distance (<1 km)	mm-level		
Proba-3	ESA	RF GPS Laser	Rough mode	Z-direction distance (Perigee) Z-direction distance (Apogee)	7.5 m | 10 m	2	No launch
			Precision mode	Z-direction distance (25–250 m) X-Y surface offset (±13 m) X-Y surface offset (±20.5 mm)	30 μm | 1 mm | 21 μm		
Darwin	ESA	Laser GPS	—	Inter-satellite baseline measurements	Submillimeter-level	5	No launch
LISA	USA (NASA)	Laser Interference	—	Interferometric ranging	10 pm	3	No launch
IRASSI	Germany (DLR)	Laser GPS	—	Interferometric ranging Altitude measurement	<5 μm <0.4 arcsec	5	No launch
FOXST	China	Vision GPS	—	Distance measurement Altitude measurement	mm-level 0.1°-level	2 × n	Under Study

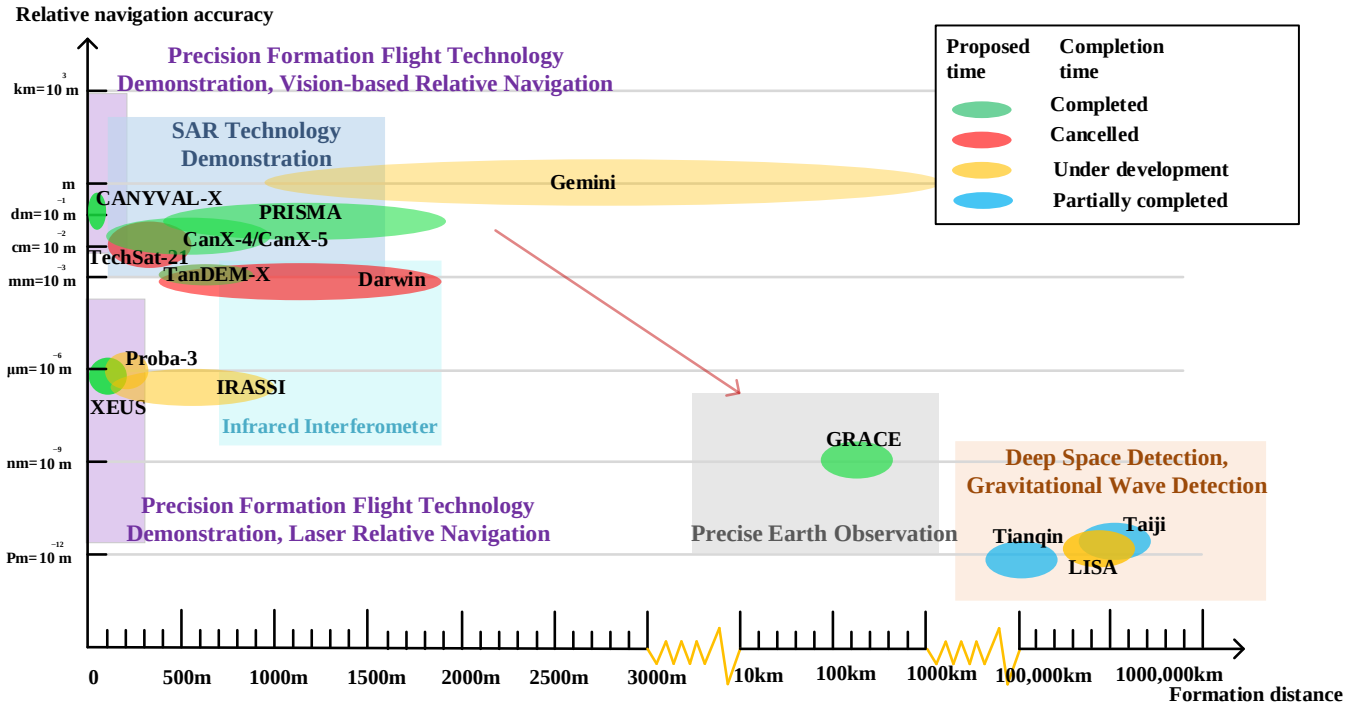

Figure 13. Relative measurement accuracy of the distributed spacecraft precision formation flying projects.

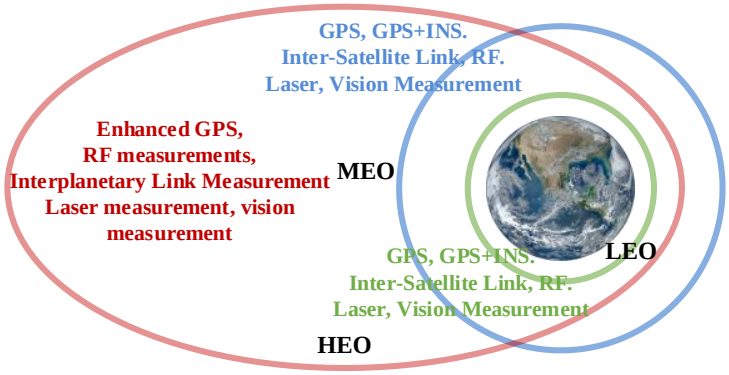

Figure 14. Measurement scheme of the inter-satellite relative state at different orbital heights.

The project background for this paper is the Focusing Optics Hard X-ray Solar Telescope (FOXST). It utilizes the precise formation of two satellites to achieve high-quality imaging of the sun's hard X-rays. The primary satellite carries a swept-in imaging optical system to converge hard X-rays, while the slave satellite is equipped with a detector system to accomplish X-ray focal plane imaging. The mission formation baseline is one hundred meters, located in the heliocentric Earth-trailing orbit, to carry out tasks. The spacecraft altitude control accuracy is required to be 1°; the relative distance control accuracy is required to be 0.1 m; measurement accuracy is required to be one order of magnitude higher than the control accuracy. The specific parameters are shown in Table 6. The Earth's trailing orbit belongs to deep space and cannot be stabilized with a GPS signal for formation. After a comprehensive investigation and analysis, combined with consideration of the future technical development direction, to control the quality of the spacecraft platform and the project budget we plan to use relatively simple visual sensors to complete the autonomous precision formation-flying task. This will be a great breakthrough in the field of deep space precision formation and is currently under study.

3. Analysis of the Characteristics of Relative State Measurement Technology

Accurate relative state information, such as relative position, relative pointing, and relative velocity, is the basis for the realization of the precise formation coordination control of spacecraft. The traditional non-autonomous method is to measure and locate a single spacecraft via a ground station. The disadvantage is that it is restricted by the ground station in the visible arc, resulting in limited measurement time, poor real-time performance, and bidirectional accuracy errors. It cannot meet the precise formation flying requirements of distributed spacecraft. Therefore, high-precision real-time state measurement technology emerges as the demand increases. The relative state measurement methods proposed include the GNSS relative measurement technology, inter-satellite radio measurement, high-precision radar measurement, optical-based autonomous measurement, and composite measurement. Autonomous measurement and non-autonomous measurement techniques are classified according to whether they need to rely on ground station equipment to complete the state measurements.

The mission objectives of different formation spacecraft projects mean that the formation shape, orbital height, and measurement accuracy have different characteristics. Figure 14 shows the navigation techniques used by the formation spacecraft at different altitudes in space orbits. After years of development, there have been many mature devices that provide inter-satellite measurement and time synchronization, such as the autonomous formation-flying sensor (AFF) [28] in the DS-3 plan, the Star Ranger star rangefinder from AeroAstro, the Stanford Pseudolite transceiver crosslink (SPTC) developed by Stanford University, the Cross Link transceiver (CLT) of the Johns Hopkins University Laboratory, and the low-power transceiver(LPT) developed by NASA.

3.1. GNSS (Global Navigation System) Signal Relative Measurement Technology

Mainstream GNSS signals include GPS (the global positioning system) in the United States, the Beidou satellite navigation system in China, Galileo in Europe, and Glonass in Russia. In this paper, GPS is used as an example for measurement analysis. GPS is an efficient and proven relative navigation method among low-orbiting satellites for distributed spacecraft precision-formation missions [29]. The formation spacecraft receives the GPS navigation signal via the GPS receiver, completes the absolute positioning, obtains the absolute speed and position, and realizes the autonomous orbit determination of the formation spacecraft. The spacecraft uses the inter-satellite link to share the GPS signal and to calculate the relative position and altitude information, so as to realize the relative state measurement of the formation flying. The principle is shown in Figure 15.

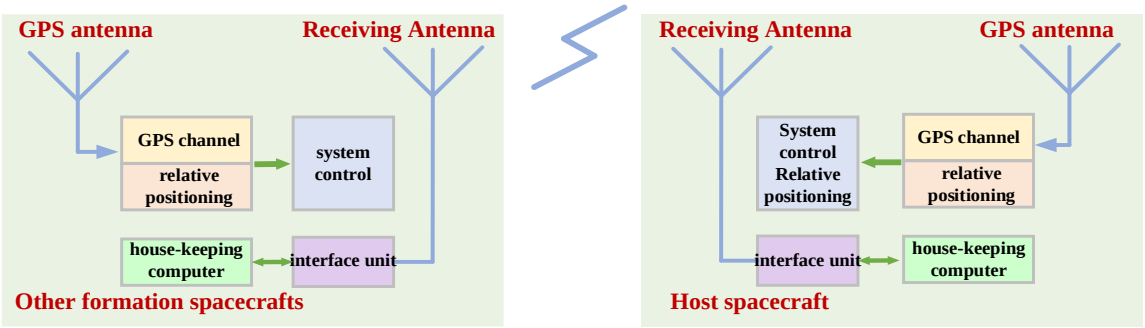

Figure 15. Principle diagram of the GPS relative measurement system.

GPS relative measurement technology is used to ascertain relative information by obtaining absolute information. Its advantages are its mature technology, it is lightweight, and has low power consumption. Its disadvantages are that its reliability and safety cannot be guaranteed in a highly dynamic space environment. It is only suitable for low–medium-orbit formation tasks and cannot effectively cover high-orbit areas. The GPS measurement algorithm is divided into the carrier phase difference (CDGPS), relative pseudo-range

difference, and relative position difference. The accuracy and scope of action are shown in Table 7.

Table 7. Performance comparison of GPS measurement methods.

Method		Technical Difficulty	Positioning Accuracy (m)	Scope of Action (km)
Position Differential		Very easy	10	100
Pseud orange differential	General pseudopitch differential	Easy	5	100
	differential smooth pseudo distance of phase	General	1	100
	Wide area differential	Very difficult	1	1000
Phase differential	Quasi-carrier phase differential	Difficulties	0.5	50
	Carrier phase differential	Very difficult	0.05	50

CDGPS [30] is currently the most precise method of GPS relative measurement. The resulting accuracy is affected by a variety of errors, some of which can be eliminated or attenuated by differentials, including GPS clock errors, GPS ephemeris errors, ionospheric delays, and receiver clock errors. Some factors that cannot be eliminated differentially include the antenna phase center error, the multipath effect error, and phase observation noise.

EXPERIMENT EARTH OBSERVING-1 (EO-1) completed an in-orbit experiment of AFF equipment for the first time. AFF used CDGPS for spacecraft distance measurement and configured multiple antennas for relative altitude measurement, as shown in Figure 16. Star Ranger also performed CDGPS for state measurement, using 12 G/15 G inter-satellite links for communication and GPS differential correction information transmission, with an accuracy of 3 mm.

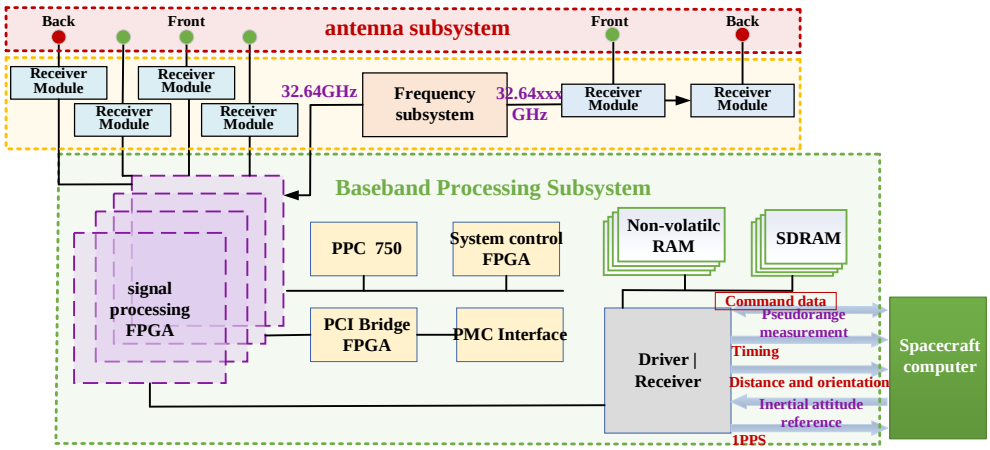

Figure 16. The AFF subsystem schematic diagram.

3.2. Laser Measurement Technology

The laser devices used for the relative state measurement of spacecraft include laser rangefinders and LiDARs [31]. The principle of laser ranging is divided into pulse measurement, phase measurement, triangulation, and interferometry. The phase ranging method obtains the distance information via the phase change of the modulated continuous light wave during round-trip propagation; the pulse ranging method obtains the distance information via the propagation time of the pulsed laser. Compared with the phase measurement, the receiver requirements of the pulse measurement are lower, the transmitter is relatively simple, and the accuracy is at dm level. The accuracy of phase measurement can reach 1 mm, and the effective distance is 100 km. The angle information is realized via four-quadrant detection, and the accuracy can attain the second level [32]. The advantages of laser measurement are its strong anti-interference ability and high precision. The disad-

vantage is that the beam is narrow and cannot be used for multi-target measurement. It is more suitable for auxiliary guidance, in combination with other measurement systems.

LiDAR acquires point-cloud data on the target surface by autonomously emitting and receiving laser beams. It reduces the complex image processing steps but also has the disadvantages of large size, high resource consumption, and high energy consumption. The current LiDARs used in autonomous relative navigation are divided into scanning and array types. The scanning type scans the field of view through the movement of the detection component, while the array type uses a fixed detection array to obtain point clouds at one moment in time. Flash LiDARs measure using the round-trip beam time, while TOF cameras measure using the phase difference. LiDAR is mainly composed of a laser-transmitting module, laser-receiving module, system control module, etc. As shown in Figure 17, the system consists of an image processing unit, a servo actuator, and a CCD to form a target capture unit. The QR four-quadrant detector is used to aim and capture the target, the optical antenna or CCD assists the radio frequency system for rough positioning, and the light-spot unit is used to measure the space angle of the target spacecraft.

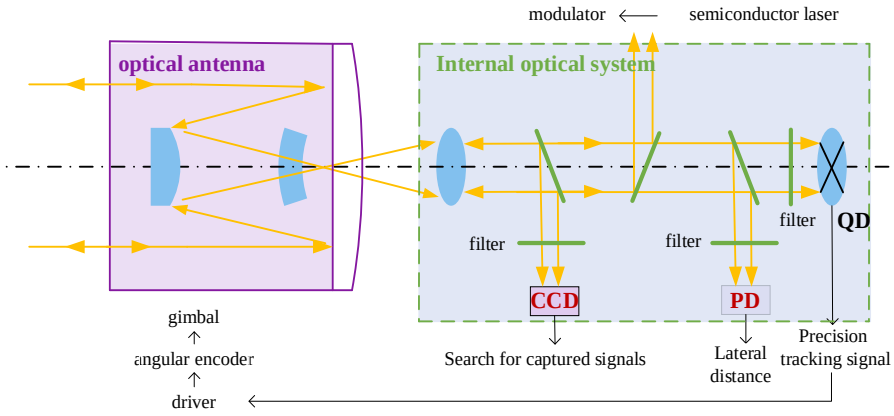

Figure 17. The spaceborne LiDAR system.

In recent years, laser interferometric ranging technology has become increasingly advanced. According to whether the frequency of the interfering laser is the same, it can be divided into two specific forms of laser interference: heterodyne and homodyne, corresponding to a dual-frequency interferometer and single-frequency interferometer, respectively. Single-frequency laser interferometers are suitable for distance measurement between targets that remain relatively stationary or that move relatively slowly. The dual-frequency laser interferometer is suitable for measuring the distance between targets with a relatively high moving speed. Both LISA and GRACE Follow-on [11] use dual-frequency laser interferometers to complete inter-satellite ranging; the performance comparisons are shown in Table 8. The dual-frequency laser interferometer detects the change in the optical path difference between the measurement arm and the reference arm, which is, essentially, a differential measurement.

Table 8. LISA and GRACE Follow-on laser-ranging system performance.

Project	Mode	Frequency Band	Accuracy	Dynamic Range	Effective Range
LISA	Outlier type	0.1–100 mHz	10 pm	±12/4 MHz	5 million km
GRACE Follow-on	Outlier type	0.2–100 mHz	80 nm	±10 MHz	220–270 km

The main components of the laser detection system of LISA include a laser interferometer measurement system, a laser source, a photodetector, and an optical telescope. The formation-satellite members are equipped with two independent measurement systems. The laser beam generated by the laser source is emitted from the optical telescope, received by the optical telescope on the formation satellite, and further input into the photodetector

and the laser interference ranging system to obtain the distance information. The LISA laser interferometric ranging system can establish the distance between two adjacent spacecraft and the pointing angle between the received laser beam and the emitted laser beam. The ranging principle is shown in Figure 18.

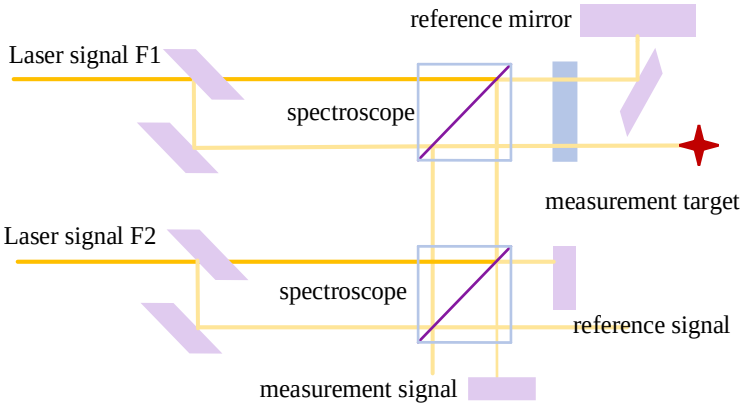

Figure 18. Schematic diagram of the LISA heterodyne interference.

The laser-ranging interferometry system of GRACE Follow-on [1] is mainly composed of optical components and phase-reading components. The optical assembly consists of a laser source, a photodetector, an optical telescope, and a fast-control mirror. The master spacecraft sends the laser beam from the optical telescope to the slave spacecraft. The laser beam is received from the slave spacecraft optical telescope, and the laser beam is forwarded in phase with the difference frequency through a heterodyne optical phase-locked loop. The main spacecraft interferes with the received retransmitted laser beam with the local reference laser beam, to form a beat frequency signal. It is further converted into an electrical signal by a photodetector. The core of the phase-reading component of the master spacecraft is a phase meter that can read the phase of the beat frequency signal and further obtain the relative pose information. The slave spacecraft is equipped with a temperature sensor and a voltage sensor for feedback control of the phase difference frequency of the laser beam. Figure 19 shows the schematic diagram of GRACE Follow-on, in which the dotted line represents the laser beam of the master star and the solid line is the laser beam forwarded from the satellite.

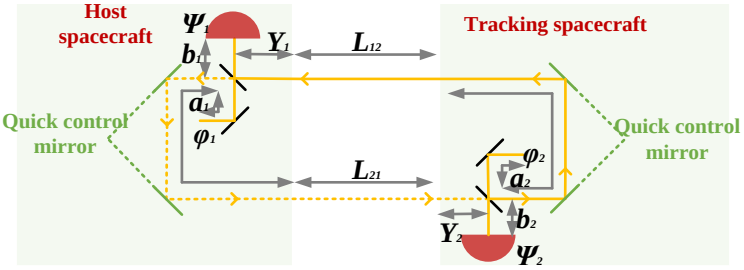

Figure 19. Schematic diagram of the GRACE Follow-on laser measurement system.

3.3. Infrared Measurement Technology

Infrared goniometric technology is a form of passive detection technology. It estimates distance, based on the attenuation of radiation intensity and changes in contrast [33]. It has a high resolution and small size, is lightweight, and has a strong anti-interference ability advantage. The basic principle of infrared measurement is to observe the target spacecraft and use image-processing technology to obtain the angular orientation information of the target spacecraft. Commonly used methods include non-modulated disk coding, modulated disk coding, linear push-broom, unit scanning, and multivariate parallel scanning. Infrared measurement can only obtain the angle information and cannot measure the relative state

of the target spacecraft alone. It needs to be combined with other active detection methods to make better use of their respective advantages and improve accuracy and continuity.

3.4. Visible Light Vision Measurement Technology

Visible light measurement is a passive detection technology, which has the advantages of wide spectral response, good linearity, and high sensitivity [34]. Visible light visual measurement technology is currently widely used in the identification of non-cooperative spacecraft, space junk, and debris [35], and is also one of the key technologies for space cooperation mission rendezvous, as well as for docking and close-range spacecraft formation flying [36]. Vision sensors such as cameras have shorter baselines and are more suitable for close-range pose measurements. Currently, visible light cameras are successfully being applied in the ETS-VII [37] and Orbital Express [38] aerospace projects. Tyvak used the composite relative measurement technology with multiple visible light and infrared cameras to demonstrate the CubeSat mission, and realized in-orbit verification of the CubeSat's formation flying.

Visible light visual measurement technology usually needs to select several feature points on the formation spacecraft to configure visible light-source beacons (usually 4 or more) [39]. The target is imaged using the optical cameras mounted on another formation spacecraft. Combined with the two-dimensional image of the target and the prior information of the optical beacon arrangement, the relative altitude and relative position information of the target spacecraft are obtained. Vision measurement techniques can be classified as monocular vision [40], binocular vision [41], and polycular vision [42] techniques. With monocular vision measurement technology, it is difficult to estimate the depth information of the optical beacon due to the limitation of the sensor, and the combination of the laser rangefinder with the depth information can better measure the space target [43]. In binocular vision measurement, the target depth information can be obtained by matching the left and right image points. Trinocular vision measurement uses the distance difference square sum algorithm to reduce the rotation axis and rotation angle errors, to obtain high-precision pose information. Visible light camera-specific sensor characteristics are shown in Table 9. The PRISMA project is equipped with a VBS camera, with a resolution of 752×582, from DTU [7]. The US Naval Research Institute uses a Bumble XB3 binocular camera, with a resolution of 1280×960 and a frame rate of 16FPS, in semi-physical experiments. After the two-dimensional image acquisition of the target is completed using the vision sensor, the stereo correspondence of the target satellite is established by using the image features. In addition, parts with regular geometric features can be projected, such as spacecraft solar panels and apogee thrusters, as a reference for the target satellite to complete feature recognition [44].

Table 9. Advantages and disadvantages of visual sensors.

Category	Advantages	Disadvantages
Monocular vision	Simple structure and small size	Lack of in-depth information
Stereo Vision	Acquisition of 3D information	Limited range and a complex algorithm
Scanning LiDAR	Easier calibration	Time-consuming
Flash LiDAR	Large detection distance range	Limited resolution and low accuracy at close range
TOF Camera	Low power consumption and compact design	Limited detection distance

The visible light vision measurement technique is practiced in the CANYVAL -X project. VisNav (vision-based navigation) [40,45] is a typical application of the visible light technique. It obtains the current measurement data through the position-sensitive diode and further calculates the estimated value of the sensor orientation. As shown in Figure 20, multiple visible light beacons of the target spacecraft are focused on the position-sensitive diode through the lens, and the relative position information of the target is obtained by using the photoelectric conversion characteristics of the sensor. This measurement technology has the disadvantages of limited applicable distance and sensitive

light conditions, but it also has the advantages of low power consumption and a small structure. Its use must be planned according to the characteristics of the task [39].

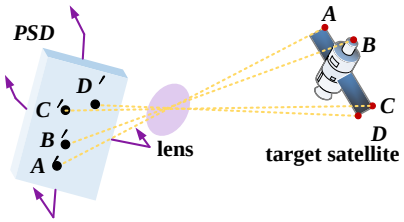

Figure 20. The VisNav sensor's relative navigation schematic.

Due to the lack of image depth in monocular vision, laser-ranging can be used for auxiliary measurement in practical solutions [43,46]. According to the existing trend analysis, the visual composite relative measurement method can fundamentally boost the advantages and may become a promising research direction in autonomous relative measurement sensors for spacecraft formations [47].

3.5. Radio-Based Autonomous Measurement Technology

Radio-ranging is an important means of measuring the relative state of formation spacecraft, also known as radio frequency ranging or GPS-like measurement technology [48]. Radio measurement offers strong continuity and high coverage. It has both communication and measurement functions in a spatial range that GNSS signals cannot cover. In addition, it supports the simultaneous communication of multiple links and can realize the functional integration design of information exchange, time synchronization, and relative state measurement. As shown in Figure 21, RF measurements make relative state measurements by deploying receivers with multiple transmit or receive antennas on the spacecraft [49].

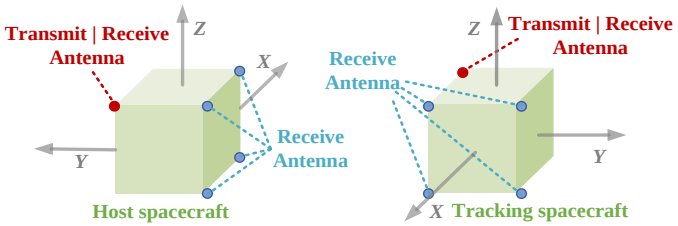

Figure 21. Principles diagram of radio state measurement.

Many devices for time synchronization and inter-satellite measurements have been developed internationally. The FFRF that was developed in the PRISMA project has a range measurement accuracy at centimeter-level and a visual angle measurement accuracy of 1° [50]; the AFF (autonomous formation-flying sensor) of the StarLight mission has a measurement accuracy of 2 cm and a relative altitude measurement accuracy of 0.025°; the KBR ranging system developed by the GRACE project is a dual-channel microwave ranging system [51]. This dual-band ranging system can eliminate the influence of the ionosphere and improve measurement accuracy. The KBR system is composed of a K-band RF-ranging sensor, a high-precision GPS receiver, a local oscillator, and a mixer for composite relative measurement, as shown in Figure 22 [52]. The satellite mixes the K/Ka signal with the local oscillation frequency, obtains the frequency difference signal for sampling and inputs it into the digital signal processing component in the GPS receiver. The corresponding channel digital phase-locked loop is used to track and solve the phase information of the frequency difference signal and transmit it to the ground for processing. The 24 GHz and 32 GHz frequencies of K/KA are used to effectively eliminate ionospheric errors [53].

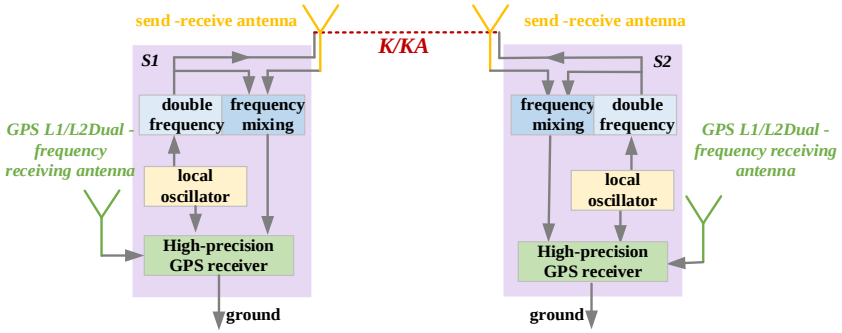

Figure 22. Structure diagram of the GRACE satellite KBR ranging system.

RF technology is relatively mature, and the current accuracy can reach the centimeter level. Its advantage is that it does not depend on external information and can be used in any orbital space. The radio frequency measurement technology adopts two-way and pseudo-code ranging. As shown in Figure 21, the transmitting and receiving antennas are configured on the master satellites and the slave satellites, and the distance from the transmitting end to the receiving end is calculated using pseudo-code and phase measurement. The master satellite is equipped with 4 receiving antennas to form a goniometer; furthermore, it uses the phase comparison method to obtain the baseline pointing of the master and slave satellites [54]. At present, the L-band radio-ranging scheme can obtain centimeter-level ranging accuracy and 0.1°-level angle-measuring accuracy. The current direction of radio-based detection methods for accuracy improvement includes the optimization of antenna distribution configuration [55] and filtering algorithm optimization [56].

3.6. Composite Relative Measurement Technology of Spacecraft Formation

GPS measurement technology is mature, small in size, and light in weight, and can provide spacecraft speed and position information [57]. RF measurement technology has high real-time accuracy and high coverage [49], but RF and GPS signals are easily blocked and interfered with. Laser measurement has high accuracy and offers system robustness [58], but the disadvantage is that the beam is narrow and requires other measurement units for auxiliary guidance. Visible-light visual measurement technology [59] is only suitable for close-range formation navigation since it needs to avoid interference from factors such as strong light and space radiation. Infrared technology [33] offers good concealment but can only provide angular information. It cannot be used as an independent measurement method. Various measurement methods offer their own advantages. In order to achieve complementary advantages in principle, more laboratories have begun to study combined measurement methods, which has greatly boosted the development of multi-sensor fusion measurement technology.

3.6.1. GPS + RF Coupling Measurement Technology

The composite relative measurement of GPS + RF [60] consists of the GPS receivers, the inter-satellite RF measurement sensor, and the relative navigation filter processor, as shown in Figure 23. The GPS receivers of the master satellites send ephemeris and observation data to the combined navigation filter and GPS orbiting processor. The GPS receivers of the slave satellites send ephemeris and observation data to the combined navigation filter through the RF sensor communication link. The GPS orbiting processor establishes the position and velocity of the primary satellites and sends them to the combined relative navigation processor for time-update solving. The RF sensor extracts high-precision inter-satellite baseline data that are further employed for combined filter updates. Combined with the relevant data of the GPS real-time orbit determination module, the GPS receiver unit, and the RF ranging module, the relative state information of the formation spacecraft is calculated via the EKF filter. The coupled GPS and RF relative measurement method can meet the real-time requirements of spacecraft precision formation measurement [61].

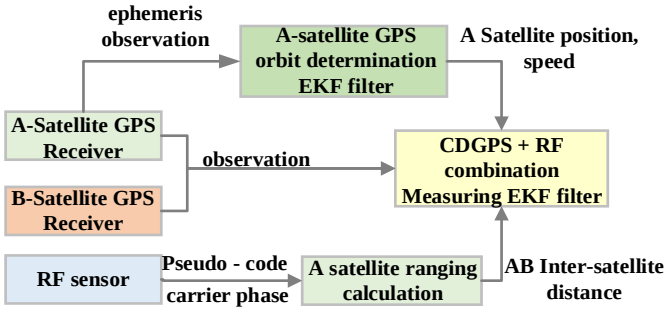

Figure 23. Schematic diagram of the GPS + RF combined relative state measurement.

3.6.2. GPS + Laser Coupling Measurement Technology

One of the technical solutions for the composite relative measurement of a GPS + laser is to use laser measurement as an auxiliary measurement. This provides sub-millimeter laser data to complement the CDGPS data. By increasing the determination accuracy of the GPS's integer ambiguity, the measurement accuracy is improved [62]. Furthermore, the measurement range of the laser, CDGPS, and the CDGPS + laser with the highest accuracy are determined through experiments, and an algorithm is designed to select the measurement method that offers the highest accuracy within the corresponding distance. The composite method has the best accuracy at 10 km.

The aim of the second solution of the GPS + laser composite relative measurement technique is to improve the problem of large altitude-estimation errors found in laser measurements over long distances. The method smooths the relative state measurement results via extended Kalman filtering. Furthermore, the laser azimuth measurement model is replaced by a GPS pseudo-range measurement single-difference model to deal with the problem of low altitude-determination accuracy. Compared with only using laser measurement, this method improves the accuracy and robustness of long-distance measurement [63].

3.6.3. GPS + Vision Coupling Measurement Technology

The aim of the GPS + visual composite relative measurement technology is to solve the problems of low visibility and the poor real-time performance of GPS signals in high orbits. The composite GPS relative measurement technology takes full advantage of the real-time capability and robustness of vision sensors. It overcomes the shortcomings of the small measurement range of vision sensors and improves the overall measurement performance [64]. The multi-sensor fusion of the relative state results, measured independently by the GPS and the vision system, improves the overall measurement accuracy, which uses a high-precision loose-coupling method [65]. It first uses the GPS orbit filter on the satellite to determine the absolute motion state of the satellite and then combines the information from the monocular camera with the GPS carrier phase observation information shared by the communication link, to obtain the relative motion state information. Finally, the relative state information is combined with orbital dynamic prediction for filtering. Obtaining high-rate state information can significantly improve the speed of solving the ambiguity of the full circumference of the carrier and gain more accurate relative state information; the process is shown in Figure 24.

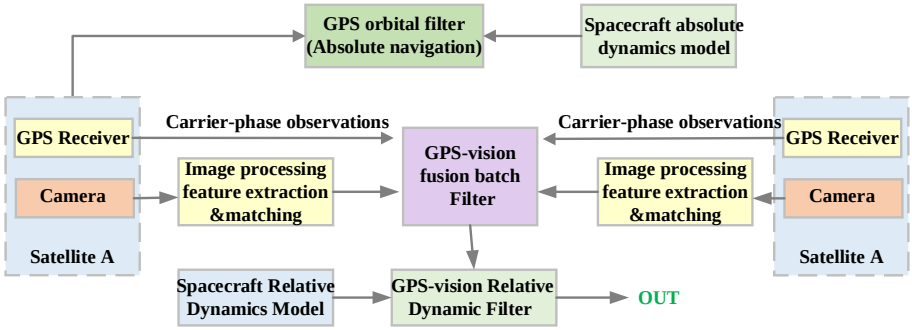

Figure 24. Schematic diagram of GPS + visual combined relative state measurement.

3.6.4. Visual Composite Close-Range Measurement Technology

Tyvak's CPOD (CubeSat Proximity Operations Demonstration) mission [66] was performed using two identical 3U (U, volume 10 × 10 × 10cm) CubeSats for formation, close-range operations, rendezvous, and docking. The measurement between satellites is completed using the PROD module [67], including a narrow field of view camera (NFOV), a docking camera, and an infrared camera (IR1/IR2), as shown in Figure 25. The image processing system reads the image from the imaging sensor and compares the a priori 3D model of the target with the image. It obtains position and pose information, using edge detection and feature extraction. Each camera can obtain a measure of the object's position and orientation. At great distances, measurements are mainly obtained using GPS and ISL. When the mission target is several kilometers away, the measurement value of NFOV occupies a larger proportion of the result. The docking camera and IR1 and IR2 account for the largest proportion of results in the short-distance measurement. At longer ranges, the target may contain only a few pixels, and the system maintains visual tracking. When the target is close to occupying more frames, pose estimation and ranging are performed. The a priori 3D models are managed by means of an on-board database, including various operations such as modification, deletion, and addition. This solves the known errors, including solar scintillation and Earth albedo effects.

Figure 25. RPOD module diagram.

Vision measurement algorithms that are based on optical image processing have high accuracy. Their disadvantages are a large number of calculations, a long processing time, and a short effective distance. In order to better utilize the advantages of vision measurement technology, combined navigation methods, such as vision-inertial navigation and vision-laser ranging, have begun to receive attention. Inertial navigation uses angular velocity information, combined with kinematic equation integration, to obtain the target altitude angle information. It can jointly filter and correct the results of visual measurement technology to gain higher precision and a more stable measurement output, as shown in Figure 26 [41]. Additionally, the pose data output of the vision measurement can correct the drift error of the inertial element and improve the accuracy by closing the loop. The laser-ranging instrument can accurately and efficiently obtain the distance information of the target spacecraft with the guidance of visual measurement technology [46,68]. It is also used as the baseline distance input of the vision measurement system for precise

measurement. This method can greatly simplify the complexity of the vision algorithm, reduce the operation time, and improve the real time and robustness of the composite measurement system.

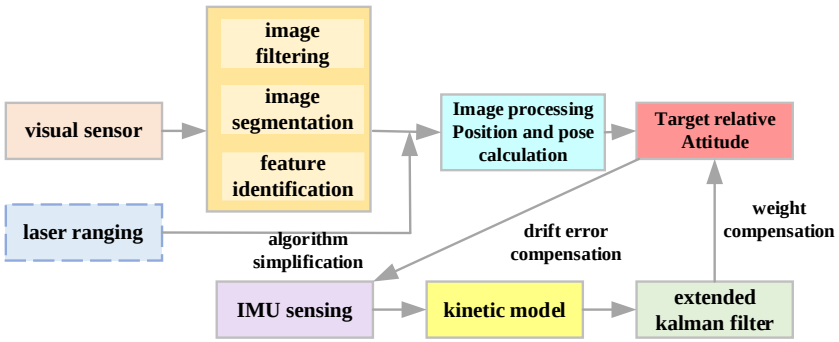

Figure 26. The schematic diagram of vision + inertial navigation + laser measurement.

3.6.5. Vision + RF Coupling Measurement Technology

Vision + RF composite relative state measurement technology is a precision measurement technology that can be applied to the deep space context. One of the current application directions is to use visual sensors as the main navigation method, while the spacecraft releases radio beacons for auxiliary observation. The radio beacon provides distance and speed information after filtering and smoothing and combines this with the sight vector of the target spacecraft to generate relatively accurate relative state measurement information [69]. With a positioning accuracy of m and an altitude measurement accuracy of 0.006°, the method can be used for precise measurements without communication, in cooperative spacecraft failure modes. Another method is to use radio to obtain the relative motion state information of the target spacecraft, in the case of communication and cooperation, and use the visual sensor to measure and obtain the relative altitude information. A filter is further designed to determine the relative position and altitude [70]; the method achieves a positioning accuracy of cm and an altitude measurement accuracy of 0.0001°.

3.6.6. Vision + Laser Coupling Measurement Technology

The visual + laser composite relative state measurement technology has strong robustness, so it is widely used in the measurement of cooperative targets in failure mode and the measurement of difficult non-cooperative targets. Laser measurements include laser ranging, laser tracking, and LiDAR. The laser tracker mainly provides visual reference values and assists the visual system in extracting specific features to complete the measurement [46]. Laser ranging is mainly used as an information source for image depth acquisition, to improve the overall algorithm accuracy and algorithm simplification [43]. The purpose of the measurement of a LiDAR point cloud and vision is to use the strong stability of the 3D laser's point cloud to make up for the poor light conditions for visual recognition. Vision sensors can compensate for the sparseness of laser point clouds and improve the overall measurement accuracy [71]. The process is shown in Figure 27. First, the stereo information of the target spacecraft is obtained via binocular camera reconstruction. The algorithm further combines the camera stereo-matching information and the radar point cloud to measure the target pose. Finally, the EKF filtering algorithm is used to obtain more accurate target spacecraft pose results. This improves the system robustness and expands the effective range.

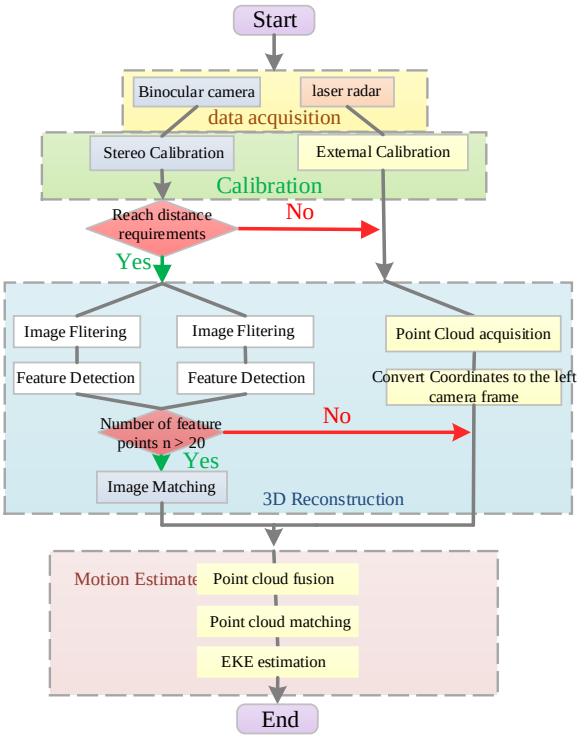

Figure 27. Schematic diagram of visual + laser coupling measurement.

3.6.7. Laser + RF Coupling Measurement Technology

Radio–laser coupling relative measurement technology is available in a variety of configurations [72]. Scheme one is to use the laser as the only measurement method, to obtain the distance and relative angle. The radio uses the laser-guided technique for cooperative measurement. Scheme two is that the radio acquires the baseline length and the laser acquires the relative angle to complete the information coupling, as shown in Figure 28.

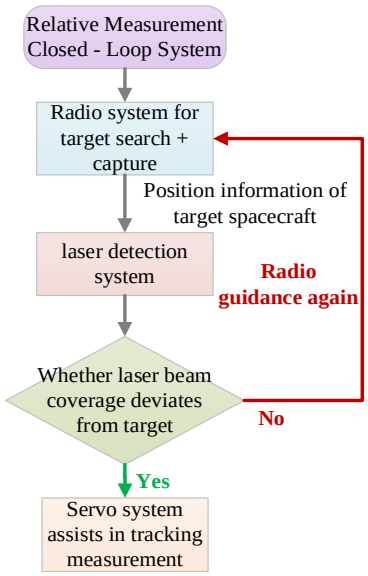

Figure 28. Radio + laser composite tracking measurement flow chart.

Scheme 1: The characteristics of wide radio coverage and its exploitation, along with radio detection, are first used to search and acquire targets. The obtained orientation information of the target spacecraft is used as the input of the laser measurement, to guide the

laser for detection. Furthermore, if the target spacecraft is still in the laser beam range after the baseline measurement is completed, the target spacecraft will continue to be tracked and measured. This action is completed using the servo mechanism and the laser transmitting and receiving system. If the target spacecraft deviates, radio guidance is performed again to complete the state measurement. Using the four-quadrant method and the principle of phase-ranging, the precision of μm-level distance measurement and arcsecond-level relative altitude measurement can be achieved. Scheme 2: First, the spacecraft is searched out and acquired using radio. The relative position and altitude of the target spacecraft are sent to the laser measurement system, and the laser is guided to measure the relative pose. At the same time, the distance measurement of the target spacecraft is realized using the radio microwave-ranging method. When the initial measurement is completed, if the target spacecraft is within the effective range of the signal, a closed-loop tracking measurement is assisted by the servo mechanism. If the target deviates from the laser beam coverage, radio guidance is performed again.

3.6.8. Laser + Infrared Coupling Measurement Technology

The principle of the coupling infrared and laser measurement technique is that infrared measurements perform target capture and guide the laser for target measurement [73]. The target search part is completed using the large-angle tracking pendulum mirror system and the infrared measurement system. The orientation information of the target spacecraft is input into the laser system, and the laser is guided to point at the target spacecraft. Since the infrared measurement accuracy is in the order of a milli-arc, the minimum guided laser-beam width is sub-milli-arc. Figure 29 shows a typical measurement system combining LiDAR and infrared measurement, including a laser rangefinder, infrared thermal imager, infrared goniometer, and information-processing components. The aim of the method is to track and locate the target spacecraft via infrared. The infrared camera obtains the angle information and the laser rangefinder obtains the distance information. The information-processing system fuses and calculates the relative position and altitude with centimeter- and arcsecond-level accuracy.

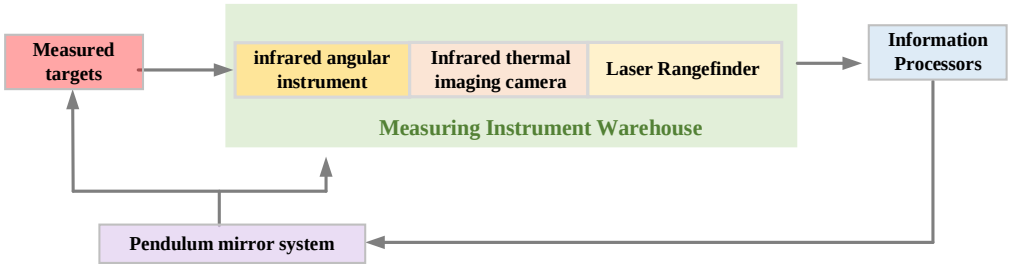

Figure 29. Schematic diagram of laser + infrared composite measurement.

3.6.9. Laser Multiple Guidance Composite Measurement Technology

It is important to consider that the radio measurement can easily achieve large-angle coverage, and the equipment is small and light. Laser measurement equipment has high precision but demands a substantial amount of energy resources. Among its characteristics is that the narrower the beam, the higher the precision. Laser multiple guidance composite measurement emerges as the demand increases. The scheme is shown in Figure 30, below [74].

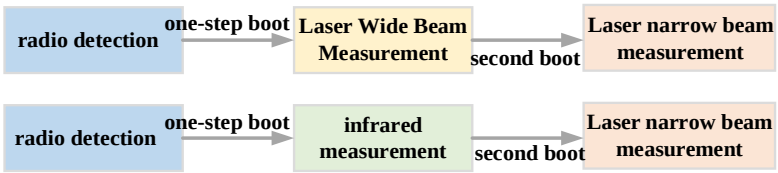

Figure 30. Flow chart of laser multiple guidance measurement.

The purpose of the measurement scheme is to first achieve a coarse acquisition of the target spacecraft through the radio characteristics of all-sky coverage. The relative position and altitude information of the target spacecraft are obtained via radio, and these are used as the guidance input of the laser wide-beam measurement system or the infrared navigation system to point at the target spacecraft. The laser wide beam or infrared measurement system is guided, to obtain more accurate position and altitude information than can be established by radio detection, and then input into the laser narrow-beam measurement system to achieve precise inter-satellite measurement.

4. Relative State Measurement Technology Trends and Optimization

4.1. Summary of the Relative State Measurement Technology Current Status

At present, the relative state measurement methods applied in the field of spacecraft precision formation flight can be divided into three groups: non-autonomous measurement technology, autonomous measurement technology, and new composite relative measurement technology. Non-autonomous measurement technology includes GNSS relative measurement technology, and autonomous measurement technology includes laser measurement, infrared measurement, radio frequency measurement, and visible light vision measurement [75,76]. The specific working range, accuracy, advantages, and disadvantages are shown in Table 10, below. As GPS relative measurements rely on GPS signals, they are only applicable to low-Earth orbits; other relative measurement methods are applicable to arbitrary orbits [77].

Table 10. Relative state measurement technology indicators.

Measurement Technology		Accuracy	Effective Range	Measurement Items	Advantages	Disadvantages
GPS	Position difference	Positioning: 10 m magnitude	>100 km	Distance, Altitude	Simple equipment, mature technology	Limited continuous navigation capability, Limited accuracy
	Pseudo-range difference	Positioning: m magnitude	<100 km			
	Carrier phase difference	Positioning: dm magnitude	<50 km			
Radio Frequency (RF)		Positioning: cm magnitude altitude determination: <1°	>30 km	Distance, Altitude	Large coverage, communication without external signal assistance	Strong anti-electromagnetic interference
Laser		Positioning: μm–nm magnitude altitude determination: <1″	m–km	Distance, Altitude	High working frequency, high precision, anti-interference	Narrow beam, needs guidance
Infrared		altitude determination: 1″	>30 km	Altitude	Simple structure, small size, strong anti-interference	Only provides angular information
Vision		Positioning: mm magnitude Altitude determination: 0.01°	<10 m	Distance, Altitude	Small equipment, simple structure	For close-range measurements only

Table 10. *Cont.*

Measurement Technology	Accuracy	Effective Range	Measurement Items	Advantages	Disadvantages
Visual Composite Measurement	Positioning: mm magnitude altitude determination: 0.01°	<500 m	Distance, Altitude	Small device size, high system robustness	Measurement accuracy decreases rapidly with increasing measurement distance
Vision + RF	Positioning: cm magnitude altitude determination: 0.0001°	50 km	Distance, Altitude	No Earth-visible arc limit	Limited precision
GPS + RF	Positioning: micron magnitude	>30 km	Distance, Altitude	Improved GPS continuity and navigation initialization process	Composite measurements require consideration of satellite platform volume, mass, resource consumption, etc.
GPS + Laser	Positioning: cm–μm magnitude altitude determination < 0.001° (10 km)	<200 km	Distance, Altitude	Improves GPS accuracy and system robustness	-
GPS + Visual	Positioning: <2 mm altitude determination: < 0.05°	5 km	Distance, Altitude	Improves GPS robustness, improving the reliability of high-orbit navigation	-
Laser + RF	Laser measurement magnitude	Laser Range	Distance, Altitude	Improves effective range while maintaining precision measurement	-
Laser + Infrared	Laser measurement magnitude	Laser Range	Distance, Altitude	Improves search capability and altitude measurement accuracy	-
Laser Multi-Guidance	Laser measurement magnitude	Laser Range	Distance, Altitude	Increased guidance speed, high robustness and accelerated measurement process	-

In this paper, the key parameters of existing international spacecraft precision formation projects are summarized. As shown in Table 6, certain conclusions can be drawn: the number of spacecraft in formation projects is increasing, and the precision requirements are becoming increasingly high. In addition, the trend of precise spacecraft formation is developing toward the ultra-long-distance precise formation and visual short-distance precise

formation; orbital distribution has also evolved from low-Earth orbit to deep space, which enables higher precision and autonomy for relative measurement technology. As shown in Table 10, influenced by mission requirements, such as orbit distribution, formation shapes, and accuracy, the focus of relative measurement technology is gradually developing from non-autonomous GNSS measurements and radio measurements to laser measurements for ultra-long-range precision formations, and visual measurements for close-range precision formations. Figure 31 shows the accuracy and valid range of different relative measurements, which can more clearly demonstrate the most advantageous intervals of different relative measurements.

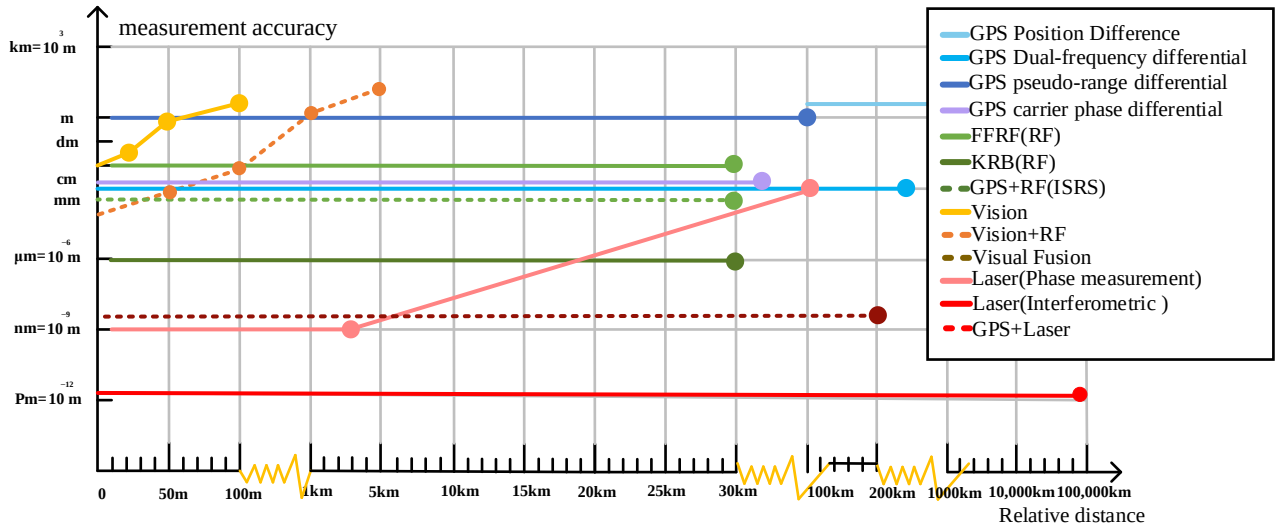

Figure 31. Accuracy comparison of the relative measurement methods.

At the same time, various subsystems influence one another in the actual project. Errors and disturbances will inevitably appear in the relative measurement system, so the robustness and reconstruction speed of the measurement technology are also important considerations. The sources of errors include the inherent properties of integrated circuits [78], space environment radiation [79], space atmospheric noise [80], etc. In addition, large disturbances may occur due to the partial failure of control systems, propulsion systems, and other subsystems, or even hardware single-particle upset [81]. These errors can be compensated by hardware anti-noise and anti-radiation design and algorithm filtering [82,83], etc. Large disturbances can be reconstructed and measured via robust algorithm control [82,84]. Different measurement technologies have different anti-interference capabilities and reconstruction times; for example, laser and infrared have strong anti-interference abilities, while vision and radio have rapid reconstruction characteristics. It is critical to select the appropriate measurement method in different application scenarios while improving the robustness of the relative measurement algorithm.

4.2. Multidisciplinary Optimized Architecture for Relative State-Measurement Payloads

The distributed spacecraft formation primarily includes spacecraft members and each spacecraft formation member includes two important components: the payload and the spacecraft platform. The payload section is the distributed primary loads used to achieve the mission, such as distributed synthetic aperture radars, distributed telescopes, and relative measurement payloads to achieve formation flying. The spacecraft platform part includes the power sub-system, structure sub-system, propulsion sub-system, and control sub-system. It is responsible for carrying the payload and ensuring the reliable operation of the spacecraft in orbit [85]. Platforms and payloads complement each other, and the improvement of the relative measurement load cannot be separated from the enhancement of the comprehensive capability of the spacecraft platform [86]. However, due to competition among the subsystems, the optimization of the payload subsystem itself tends to

compromise the performance of the platform subsystem. In order to improve the accuracy as well as the robustness of the relative measurement payload, one cannot start only from the optimization goal of the load subsystem but should instead start from the overall function of the formation. The overall design of a distributed spacecraft formation is a typical multi-disciplinary design optimization problem, with complex coupling relationships. As shown in Figure 32, this paper proposes a method architecture to select and optimize the relative measurement technologies of spacecraft, based on the overall design view of spacecraft formation flying. Under the premise of considering the disciplinary coupling and competitiveness among subsystems, such as relative measurement payloads, spacecraft platforms, and several design issues, such as formation shapes, distributed spacecraft platforms, and spacecraft loads, the differences between them should be fully considered. Multiple design goals should be effectively coordinated, constraints should be designed among distributed spacecraft subsystems, and the optimal balance point should be sought. While ensuring the overall optimization of the system, the selection analysis and optimization of the relative measurement load are completed. This approach offers distinct advantages over serial optimization methods that do not consider the coupling of other systems [87]. This provides a new approach to the relative state measurement payload optimization of distributed spacecraft formation flying in the future.

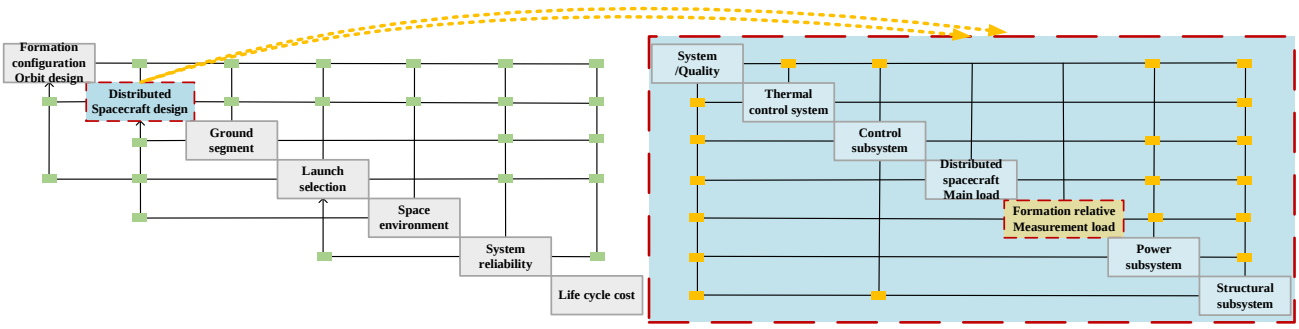

Figure 32. Design structure matrix of the overall design problem of distributed spacecraft formation flying.

The multidisciplinary design optimization method, which was first proposed by the mathematician J. Sobieszczanski-Sobieski in 1982, is an engineering method that can take into account the coupling of different disciplines or subsystems and that aims to solve the optimal design of complex systems [88]. It has been successfully applied to launch vehicle optimization design [86], satellite overall design [89], satellite constellation design [90,91], etc. The overall design of the distributed spacecraft in formation flying is mainly based on the design team's initial design solutions and using manual experience; the subsystems are constantly coordinated to obtain a proposal that meets the mission requirements. The artificial experience method cannot take into account many of the constraints and coupling relationships between subsystems and cannot realize the optimization of various design schemes in a short time. This presents the shortcomings of a long cycle and a high cost [87]. This is highly unfavorable for the relative state measurement payload selection and optimization described in this paper. Therefore, for the first time, this paper proposes a multidisciplinary optimization framework to select and optimize the relative state measurement payloads of distributed spacecraft formation flying. In order to improve the accuracy and robustness of relative state measurement payloads, based on the overall trade-off of the formation design and the comprehensive consideration of the coupling relationship between subsystems, this paper proposes a multidisciplinary design optimization architecture by which to select relative state measurement payloads and optimize their performance parameters to find the best design solution.

The coupling relationship between the distributed spacecraft formation flying subsystems is shown in the design structure matrix in Figure 32. The boxes represent the

subsystem modules and the horizontal and vertical lines are the input and output of each subsystem module; the nodes symbolize the coupling and dependencies between the subsystems.

The key issues of overall formation design decomposed by the design structure matrix (DSM) in this paper are allocated to the system and subsystem levels for optimization, as shown in Figure 32. The system-level target selection can be decided according to the mission requirements and the designer's focus. The architecture can process coupled sub-problems, such as the formation configuration design, load performance, platform performance, and spacecraft cost analysis, both in parallel and independently, to solve the coupling and competition effects between sub-problems. Under the given design constraints, at the system level, each discipline independently completes the analysis and design of this discipline and returns the design results to the system level. Finally, the system level is coordinated and optimized to obtain the optimal design that meets all the requirements. An optimal design that achieves a comprehensive balance of performance, cost, reliability, and maintainability is obtained; then, the type selection and parameter optimization of relative measurement payloads are conducted, as shown in Figure 33. At present, the researchers in this paper have used the visual monocular sensor, combined with multi-disciplinary collaborative optimization, to develop the ultra-precision short-range visual spacecraft formation flying project.

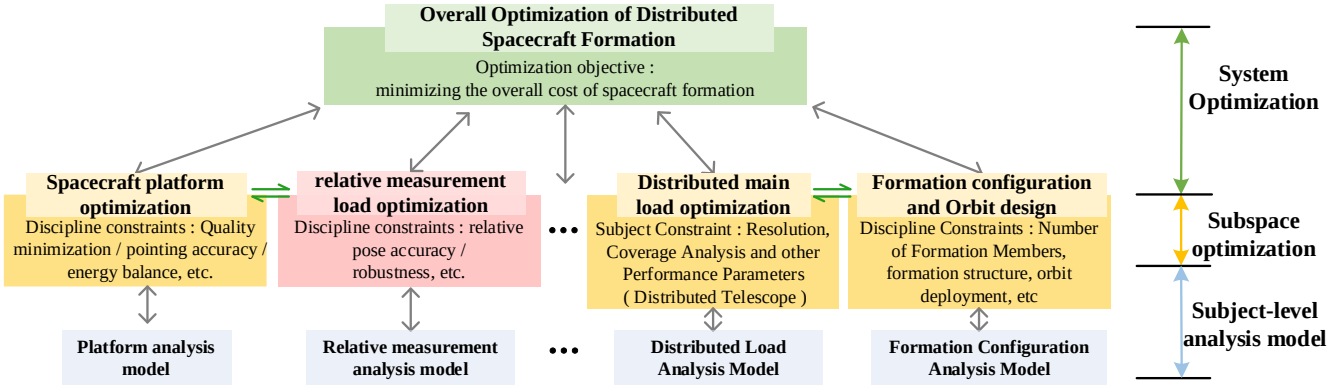

Figure 33. Multidisciplinary optimization structure diagram of the overall design of distributed spacecraft formation flying.

4.3. Development Trend

This paper reviewed the key parameters of the existing international spacecraft precision formation engineering projects. As shown in Table 10, it can be concluded that the accuracy requirements of formation projects are becoming increasingly high, and the number of formation spacecraft is also increasing. In addition, the precise formations of spacecraft have developed according to two aspects: ultra-long-distance precise formation and visual short-range precise formation; the orbit distribution is likewise evolving, from near-Earth orbit to deep space. This poses higher requirements for the precision and autonomy of relative state measurement technology. As shown in Table 10, when affected by orbit distribution, formation configuration, and accuracy, relative state measurement technology has gradually developed from non-autonomous GPS and radio measurement to laser and visual measurements. The development trend of specific relative measurement technology is as follows.

Sensor fusion for spacecraft relative state measurement presents a promising development direction [92,93]. Table 10 shows some of the data for the precision dimension. The mainstream composite relative state measurement techniques can be divided into two approaches: the tight coupling approach and the loose coupling approach. The tight coupling approach usually combines heterogeneous data from different measurement methods at the algorithm level to produce the final measurement result. Wide coupling is used to

select a method with higher measurement accuracy or to combine simple processing as the final measurement result at different range stages. Tight coupling can often improve specific dimensions such as accuracy, real-time characteristics, and autonomy. The results of wide coupling depend on the accuracy and real-time characteristics of each measurement method. The advantage of this approach is that it has better robustness and can make full use of the advantages of each measurement method. The focus of fusion technology is to guarantee the best accuracy while ensuring an optimal spacecraft platform; that is, to establish how to use sensor fusion with the fewest resources and lowest cost consumption to achieve the best accuracy, real-time characteristics, robustness, and other indicators. This can provide more possibilities for formation flying missions, rather than just pursuing accuracy metrics.

The intelligence of the relative state measurement of distributed spacecraft formation flying is also a promising development direction. Due to limitations in measuring and controlling the visible arc, there is a limited amount of time in which ground personnel can intervene in decision-making. This makes intelligence regarding the formation system even more important. With the development of artificial intelligence technology, people are no longer satisfied with a fixed, traditional operating mode but instead hope to improve the formation's own system through autonomous learning. For example, Yue-Hua Cheng completed the allocation of radio resources to satellites via reinforcement learning, and accomplished the assignment of conflicting mission objectives [94]; Ferreira adopted a learning method to take the task reward and control cost as dual optimization objectives and obtained an optimal reconfiguration strategy for the spacecraft altitude control system [95]; Davis solved the difficulty of the mutual visual recognition of formation satellites by using an unsupervised learning architecture [96]. Combining information data from relative state measurement, communication, mission-planning, etc., enables the formation members to make intelligent decisions. The system no longer relies on the inherent relative state measurement procedure to realize formation and instead adopts an intelligent learning method to complete relative identification measurements, as well as task objective and self-control optimization [97,98].

The precision formation flying of spacecraft as an aerospace engineering mission is inevitably subject to errors or failures in actual measurement and control. Robust relative measurement and formation control under partial failure is also an advantageous development direction. The stability of formation measurement is mainly achieved through two aspects, the optimized design of hardware against radiation and noise [99,100], and the algorithm of robust measurement and control under partial failure [82,83,101].

The software-defined distributed spacecraft formation flying relative state measurement refers to the calculation of the center and the software as a means to complete the measurement function [102]. Functions such as communication and relative measurement load, which are traditionally realized by subsystems, are realized via software [103]. From the overall perspective of the spacecraft, the relative measurement load, control subsystems, and other actuators are connected, as a whole, through software. It relies on an efficient computer processing platform and can realize plug-and-play measurement loads through an open software architecture. By loading application software on demand and quickly reconfiguring the spacecraft, it is possible to flexibly add or remove the formation members.

5. Conclusions

This paper analyzes the typical tasks in the precise formation of distributed spacecraft. At present, the development of related mission requirements is diversified, which is reflected in the formation's shape, formation trajectory, detection performance, etc. In addition, laser ultra-long-distance precision formation and visual short-range precision formation are hot topics in mission development. Formation autonomy and robustness requirements are gradually increasing. The orbital distribution of formations is also gradually developing, from near-Earth orbit to deep space, which poses greater technical challenges

in precision spacecraft relative state measurement technology, relative navigation and control technology, and measurement sensor hardware manufacturing.

The field of distributed spacecraft formation measurement can be divided into non-autonomous measurement technology, autonomous measurement technology, and new composite relative measurement technology. This paper summarizes the specific working principles, effective range, accuracy, advantages, and disadvantages of GPS relative measurement, laser measurement, infrared measurement, radio frequency measurement, visual measurement, and new composite measurement. In response to the trend of overall space mission optimization, a multidisciplinary optimization architecture is proposed, to address the selection and optimization of measurement loads for distributed spacecraft formation flying. This can effectively resolve the competition relationship between the subsystems of the formation spacecraft. According to the mission requirements, the optimization of the relative measurement load is completed on the premise of ensuring the optimization of the spacecraft platform, and a balance between indicators and resource allocation is achieved. This completes the coordinated optimization of the platform and the payload while considering the rationalization of the weight, volume, and resource allocation of the satellite platform. Finally, an overview of potential development directions is outlined: spacecraft relative state measurement sensor fusion, distributed spacecraft formation measurement intelligence, robust relative measurement under partial faults, and software-defined distributed spacecraft formation measurement.

Author Contributions: Conceptualization, Z.Z. and L.D.; methodology, Z.Z. and L.D. software, n/a; validation, n/a; formal analysis, Z.Z., Y.Q. and D.L.; investigation, Z.Z., J.F., L.C. and Y.Q.; resources, Z.Z., L.D., L.C. and D.L.; data curation, Y.Q.; writing—original draft preparation, Z.Z.; writing—review and editing, Z.Z.; visualization, Z.Z. and J.F.; supervision, L.C.; project administration, L.D.; funding acquisition, D.L. All authors have read and agreed to the published version of the manuscript.

Funding: This research was funded by Formation Flying Focusing Optics Hard X-ray Solar Telescope, grant number XDA15016800.

Institutional Review Board Statement: Not applicable.

Informed Consent Statement: Not applicable.

Data Availability Statement: Not applicable.

Conflicts of Interest: The authors declare no conflict of interest.

References

1. Goswami, S.; Francis, S.P.; Bandikova, T.; Spero, R.E. Analysis of GRACE Follow-On Laser Ranging Interferometer Derived Inter-Satellite Pointing Angles. *IEEE Sens. J.* **2021**, *21*, 19209–19221. [CrossRef]
2. Zink, M.; Moreira, A.; Hajnsek, I.; Rizzoli, P.; Wessel, B. TanDEM-X: 10 Years of Formation Flying Bistatic SAR Interferometry. *IEEE J. Sel. Top. Appl. Earth Obs. Remote Sens.* **2021**, *14*, 3546–3565. [CrossRef]
3. Hughes, M.; Norris, S. An Overview of the Technology Satellite of the 21st Century (TechSat 21) Program. In *Smaller Satellites: Bigger Business?* Springer: Dordrecht, The Netherlands, 2002; Volume 6, pp. 381–382. [CrossRef]
4. Das, A.; Cobb, R. TechSat 21—Space Missions Using Collaborating Constellations of Satellites. In Proceedings of the 12th AIAA/USU Conference on Small Satellites, Logan, UT, USA, 31 August–11 September 1998.
5. Cockell, C.S.; Herbst, T.; Léger, A.; Absil, O.; Beichman, C.; Benz, W.; Brack, A.; Chazelas, B.; Chelli, A.; Cottin, H. Darwin—An Experimental Astronomy Mission to Search for Extrasolar Planets. *Exp. Astron.* **2009**, *23*, 435–461. [CrossRef]
6. Grelier, T.; Guidotti, P.Y.; Delpech, M.; Harr, J.; Leyre, X. Formation Flying Radio Frequency Instrument: First Flight Results from the PRISMA Mission. In Proceedings of the Satellite Navigation Technologies & European Workshop on Gnss Signals & Signal Processing, Toulouse, France, 8–9 December 2011.
7. Persson, S.; Veldman, S.; Bodin, P. PRISMA—A formation Flying Project in Implementation Phase. *Acta Astronaut.* **2009**, *65*, 1360–1374. [CrossRef]
8. Parmar, A.N.; Hasinger, G.; Arnaud, M.; Barcons, X.; Barret, D.; Blanchard, A.; Boehringer, H.; Cappi, M.; Comastri, A.; Courvoisier, T.; et al. XEUS—The X-ray Evolving Universe Spectroscopy Mission. In Proceedings of the Conference on Space Telescopes and Instrumentation II: Ultraviolet to Gamma Ray, Orlando, FL, USA, 15 June 2006.
9. Arnaud, M.; Barcons, X.; Barret, D.; Bautz, M.; Bellazzini, R.; Bleeker, J.; Böhringer, H.; Boller, T.; Brandt, W.N.; Cappi, M.; et al. XEUS: The Physics of the Hot Evolving Universe. *Exp. Astron.* **2009**, *23*, 139–168. [CrossRef]

10. Jennrich, O. LISA Technology and Instrumentation. *Class. Quantum Gravity* **2009**, *26*, 153001–153032. [CrossRef]
11. Schütze, D.; Stede, G.; Müller, V.; Gerberding, O.; Mahrdt, C.; Sheard, B.; Heinzel, G.; Danzmann, K. LISA-like Laser Ranging for GRACE Follow-on. Proceedings of 9th LISA Symposium, Paris, France, 21–25 May 2012.
12. Stephens, M.; Craig, R.; Leitch, J.; Pierce, R.; Nerem, R.; Bender, P.; Loomis, B. Demonstration of an Interferometric Laser Ranging System for a Follow-On Gravity Mission to GRACE. In Proceedings of the 2006 IEEE International Symposium on Geoscience and Remote Sensing, Denver, CO, USA, 31 July–4 August 2006.
13. Shahzad, M.W.; Burhan, M.; Ang, L.; Ng, K.C. Energy-water-Environment Nexus Underpinning Future Desalination Sustainability. *Desalination* **2017**, *413*, 52–64. [CrossRef]
14. Watkins, M.; Flechtner, F.; Morton, P.; Webb, F. Status of the GRACE Follow-On Mission. *Egu Gen. Assem.* **2014**, *141*, 117–121. [CrossRef]
15. Orr, N.G.; Eyer, J.K.; Larouche, B.P.; Zee, R.E. Precision Formation Flight: The Can X-4 and Can X-5 Dual Nanosatellite Mission. In Proceedings of the Esa Special Publication, Karlsruhe, Germany, 15–17 September 2008.
16. Landgraf, M.; Mestreau-Garreau, A. Formation Flying and Mission Design for Proba-3. *Acta Astronaut.* **2013**, *82*, 137–145. [CrossRef]
17. Llorente, J.S.; Agenjo, A.; Carrascosa, C.; de Negueruela, C.; Mestreau-Garreau, A.; Cropp, A.; Santovincenzo, A. PROBA-3: Precise Formation Flying Demonstration Mission. *Acta Astronaut.* **2013**, *82*, 38–46. [CrossRef]
18. Kurahashi, T.; Menini, A. TanDEM-X: A Satellite Formation for High-Resolution SAR Interferometry. *IET* **2009**, *45*, 3317–3341. [CrossRef]
19. Moreira, A.; Krieger, G.; Hajnsek, I.; Hounam, D.; Settelmeyer, E. TanDEM-X: A TerraSAR-X Add-On Satellite for Single-Pass SAR Interferometry. In Proceedings of the Geoscience and Remote Sensing Symposium, IGARSS '04, Anchorage, AK, USA, 20–24 September 2004.
20. Guarnieri, A.M.; Tebaldini, S.; Rocca, F.; Broquetas, A. GEMINI: Geosynchronous SAR for Earth Monitoring by Interferometry and Imaging. In Proceedings of the Geoscience & Remote Sensing Symposium, Munich, Germany, 22–27 July 2012.
21. Park, J.P.; Park, S.Y.; Lee, K.; Oh, H.J.; Kim, T.H. Mission Analysis and CubeSat Design for CANYVAL-X Mission. In Proceedings of the 14th International Conference on Space Operations, Daejeon, Korea, 16–20 May 2016.
22. Jun, L.; Linghao, A.; Yanli, A.; Zicong, A.; Weigang, B.; Yanzheng, B.; Jiahui, B.; Bin, C.; Wenbo, C.; Chen, C.; et al. A Brief Introduction to the TianQin project. *Acta Sci. Nat. Univ. Sunyatseni* **2021**, *60*, 1–19.
23. Hu, Y.; Mei, J.; Luo, J. TianQin Project and International Collaboration. *Chin. Sci. Bull.-Chin.* **2019**, *64*, 2475–2483. [CrossRef]
24. Liu, H.S.; Luo, Z.R.; Sha, W. In-Orbit Performance of the Laser Interferometer of Taiji-1 Experimental Satellite. *Int. J. Mod. Phys. A* **2021**, *36*, 2140004. [CrossRef]
25. Hu, Z.; Wang, P.; Deng, J.; Cai, Z.; Wang, Z.; Wang, Z.; Yu, J.; Wu, Y.; Kang, Q.; Li, H.; et al. The Drag-Free Control Design and in-Orbit Experimental Results of "Taiji-1". *Int. J. Mod. Phys. A* **2021**, *36*, 2140019. [CrossRef]
26. Buinhas, L.; Philips-Blum, M.; Frankl, K.; Pany, T.; Eissfeller, B.; Forstner, R. Formation Operations and navigation Concept Overview for the IRASSI space Interferometer. In Proceedings of the 2018 IEEE Aerospace Conference, Big Sky, MT, USA, 3–10 March 2018; IEEE: Big Sky, MT, USA, 2018; pp. 1–16.
27. Buinhas, L.; Linz, H.; Philips-Blum, M.; Foerstner, R. iSCOUT: Science-Task Planning and Formation Maneuver Design for the IRASSI Space Interferometer. *Adv. Space Res.* **2021**, *67*, 3840–3867. [CrossRef]
28. Scharf, D.P.; Hadaegh, F.Y.; Kang, B.H. A Survey of Spacecraft Formation Flying Guidance and Control (part 1): Guidance. In Proceedings of the American Control Conference, Boston, MA, USA, 30 June–2 July 2004.
29. Yuan, J.; Jia, H.; Fang, Q. Application of GPS to space Vehicles: Analysis of Space environment and Errors. *IEEE Aerosp. Electron. Syst. Mag.* **1998**, *13*, 25–30. [CrossRef]
30. Montenbruck, O.; Ebinuma, T.; Lightsey, E.G.; Leung, S. A Real-Time Kinematic GPS Sensor for Spacecraft Relative Navigation. *Aerosp. Sci. Technol.* **2002**, *6*, 435–449. [CrossRef]
31. Opromolla, R.; Fasano, G.; Rufino, G.; Grassi, M. Uncooperative Pose Estimation with a LIDAR-Based System. *Acta Astronaut.* **2015**, *110*, 287–297. [CrossRef]
32. Gao, P.; Zheng, Y. Characters of Laser Ranging on Inter-Satellite Relative Position Measurement. In Proceedings of the International Conference on Recent Advances in Space Technologies, Istanbul, Turkey, 14–16 June 2007.
33. Zhu, Y.; Sun, Y.; Zhao, W.; Huang, B.; Wu, L. Relative navigation for Autonomous Aerial Refueling Rendezvous Phase. *Optik* **2018**, *174*, 665–675. [CrossRef]
34. Erkec, T.Y.; Hajiyev, C. Vision-Based Approaches of the Small Satellites Relative Navigation. *Wseas Trans. Comput. Res.* **2021**, *9*, 13–20. [CrossRef]
35. Qian, F.; Zhu, Z.H.; Quan, P.; Hou, X. Relative State and Inertia Estimation of Unknown Tumbling Spacecraft by Stereo Vision. *IEEE Access* **2018**, *6*, 54126–54138. [CrossRef]
36. Sabatini, M.; Palmerini, G.B.; Gasbarri, P. A testbed For Visual Based Navigation and Control during Space Rendezvous Operations. *Acta Astronaut.* **2015**, *117*, 184–196. [CrossRef]
37. Yoshida, K. *Engineering Test Satellite VII Flight Experiments for Space Robot Dynamics and Control: Theories on Laboratory Test Beds Ten Years Ago, Now in Orbit*; Springer: Berlin/Heidelberg, Germany, 2003; Volume 22, pp. 321–335. [CrossRef]
38. Shoemaker, J.; Wright, M. Orbital Express Space Operations Architecture Program. *Proc. SPI—Int. Soc. Opt. Eng.* **2004**, *5088*, 1–9. [CrossRef]

39. Jeong, J.; Kim, S.; Suk, J. Parametric Study of Sensor Placement for Vision-Based Relative Navigation System of Multiple Spacecraft. *Acta Astronaut.* **2017**, *141*, 36–49. [CrossRef]
40. Pan, H.; Huang, J.; Qin, S. High Accurate Estimation of Relative Pose of Cooperative Space Targets Based on Measurement of Monocular Vision Imaging. *Opt.-Int. J. Light Electron Opt.* **2014**, *125*, 3127–3133. [CrossRef]
41. Segal, S.; Carmi, A.; Gurfil, P. Stereovision-Based Estimation of Relative Dynamics Between Noncooperative Satellites: Theory and Experiments. *IEEE Trans. Control. Syst. Technol.* **2014**, *22*, 568–584. [CrossRef]
42. An, S.; Haodong, P.; Huixian, D. Trinocular Stereo Visual Measurement Method for Spatial Non-Cooperative Target. *Acta Opt. Sin.* **2021**, *41*, 0615001. [CrossRef]
43. Liu, Y.; Xie, Z.; Liu, H. Three-Line Structured Light Vision System for Non-Cooperative Satellites in Proximity Operations. *Chin. J. Aeronaut.* **2020**, *33*, 1494–1504. [CrossRef]
44. Ning, M.; Zhang, S.; Wang, S. A Non-Cooperative Satellite Feature Point Selection Method for Vision-Based Navigation System. *Sensors* **2018**, *18*, 854. [CrossRef]
45. Christian, J.A.; Robinson, S.B.; D'Souza, C.N.; Ruiz, J.P. Cooperative Relative Navigation of Spacecraft Using Flash Light Detection and Ranging Sensors. *J. Guid. Control. Dyn.* **2014**, *37*, 452–465. [CrossRef]
46. Peng, J.; Xu, W.; Yuan, H. An Efficient Pose Measurement Method of a Space Non-Cooperative Target Based on Stereo Vision. *IEEE Access* **2017**, *5*, 22344–22362. [CrossRef]
47. Gao, X.; Liang, B.; Du, X.; Xu, W. Pose measurement of large Non-Cooperative Satellite Using Structured Light Vision Sensor. In Proceedings of the 2012 IEEE International Conference on Information Science and Technology, Wuhan, China, 23–25 March 2012. [CrossRef]
48. He, D.L.; Cao, X.B. Relative States Autonomous Determination of Satellites Formation Flying. In Proceedings of the 2006 International Conference on Machine Learning and Cybernetics, Dalian, China, 13–16 August 2006; pp. 742–748.
49. Weiqing, M.; Liu, R.; Xinxin, Y.; Kamel, E. Analysis of Precision Estimation of RF Metrology in Satellite Formation Flying. In Proceedings of the 2015 International Conference on Wireless Communications & Signal Processing (wcsp), Nanjing, China, 15–17 October 2015; IEEE: New York, NY, USA, 2015.
50. Grelier, T.; Guidotti, P.Y.; Delpech, M.; Harr, J.; Leyre, X. Formation Flying Radio Frequency Instrument: First Flight Results from the PRISMA Mission. In Proceedings of the Satellite Navigation Technologies & European Workshop on Gnss Signals & Signal Processing, Noordwijk, The Netherlands, 8–10 December 2010.
51. Lee, C.K.; Han, S.C.; Bilitza, D.; Chung, J.K. Validation of International Reference Ionosphere Models Using in Situ Measurements from GRACE K-Band Ranging System and CHAMP Planar Langmuir Probe. *J. Geod.* **2011**, *85*, 921–929. [CrossRef]
52. Wang, F. *Study on Center of Mass Calibration and K-Band Ranging System Calibration of the Grace Mission*; The University of Texas at Austin: Ann Arbor, MI, USA, 2003.
53. Thevenet, J.-B.; Grelier, T. Formation Flying Radio-Frequency Metrology Validation and Performance: The PRISMA case. *Acta Astronaut.* **2013**, *82*, 2–15. [CrossRef]
54. Mo, S.; Jin, X.; Lin, C.; Zhang, W.; Xu, Z.; Jin, Z. Multi-Satellite Relative Navigation Scheme for Microsatellites Using Inter-Satellite Radio Frequency Measurements. *Sensors* **2021**, *21*, 3725. [CrossRef]
55. Mu, W.; Liu, R.; Wang, Z.; Liu, Y. Antenna Configuration Method for RF Measurement Based on DOPs in Satellite Formation Flying. *Int. J. Aerosp. Eng.* **2018**, *2018*, 4216971. [CrossRef]
56. Liu, C.; An, J.; Zhang, R. Zhang Radio-Based Relative State Measurement Algorithm for Micro-Nano Satellite Formation. In Proceedings of the 2019 IEEE 2nd International Conference on Electronics Technology (ICET), 10–13 May 2019; Chengdu, China; pp. 13–19.
57. Peng, Y.X.; Scales, W.A.; Edwards, T.R. GPS-Based Satellite Formation Flight Simulation and Applications to Ionospheric Remote Sensing. *Navigation* **2020**, *67*, 3–21. [CrossRef]
58. Dirkx, D.; Prochazka, I.; Bauer, S.; Visser, P.; Noomen, R.; Gurvits, L.I.; Vermeersen, B. Laser and radio tracking for planetary science missions—A comparison. *J. Geod.* **2019**, *93*, 2405–2420. [CrossRef]
59. Sun, W.; Chen, L.; Liu, K. Research on Vision-Based Autonomous Navigation Algorithm for RVD between Spacecrafts. *JSCSE* **2012**, *2*, 1–12. [CrossRef]
60. Fan, G.Q.; Wang, W.; Xiao-Ning, X.I. Application of GPS and Like-GPS Carrier Phase in States Measurement of Formation Constellation. *Comput. Simul.* **2006**, *1*, 44–47. [CrossRef]
61. Allende-Alba, G.; D'Amico, S.; Montenbruck, O. Radio-Frequency Sensor Fusion for Relative Navigation of Formation Flying Satellites. *Int. J. Space Sci. Eng.* **2015**, *3*, 129–147. [CrossRef]
62. Kang, D.-E.; Park, S.-Y.; Son, J. Characteristics of Relative Navigation Algorithms Using Laser Measurements and Laser-GPS Combined Measurements. *J. Astron. Space Sci.* **2018**, *35*, 287–293. [CrossRef]
63. Oh, H.; Park, H.-E.; Lee, K.; Park, S.-Y.; Park, C. Improved GPS-Based Satellite Relative Navigation Using Femtosecond Laser Relative Distance Measurements. *J. Astron. Space Sci.* **2016**, *33*, 45–54. [CrossRef]
64. Barreau, V.; Priot, B.; Calmettes, V.; Sahmoudi, M. A New Approach for Deep Integration of GNSS and Vision-Aided MEMS IMU. In Proceedings of the Ion Gnss, Portland, OR, USA, 21–24 September 2010.
65. Wang, X.; Shao, X.; Gong, D.; Duan, D. GPS/VISNAV Integrated Relative Navigation and Attitude Determination System for Ultra-Close Spacecraft Formation Flying. *J. Syst. Eng. Electron.* **2011**, *22*, 9. [CrossRef]

66. Bowen, J.; Tsuda, A.; Abel, J.; Villa, M. CubeSat Proximity Operations Demonstration (CPOD) Mission Update. In Proceedings of the 2015 IEEE Aerospace Conference, Big Sky, MT, USA, 7–14 March 2015.
67. Roscoe, C.; Westphal, J.J.; Mosleh, E. Overview and GNC design of the CubeSat Proximity Operations Demonstration (CPOD) Mission. *Acta Astronaut.* **2018**, *153*, 410–421. [CrossRef]
68. Giubilato, R.; Chiodini, S.; Pertile, M.; Debei, S. MiniVO: Minimalistic Range Enhanced Monocular System for Scale Correct Pose Estimation. *IEEE Sens. J.* **2020**, *20*, 11874–11886. [CrossRef]
69. Jing, Y.; Zhu, S.; Wang, L. Autonomous Optical Navigation Approach Aided by Radio Beacon for Deep Space Spacecraft. In Proceedings of the 2016 Chinese Control and Decision Conference, Yinchuan, China, 28–30 May 2016.
70. Wang, X.; Shao, X.; Gong, D.; Duan, D. Radio/VISNAV Integrated Navigation System for Autonomous Spacecraft Rendezvous Using Two-Order Filter. In Proceedings of the 8th World Congress on Intelligent Control and Automation, Jinan, China, 6–9 July 2010; pp. 1735–1740.
71. Peng, J.; Xu, W.; Liang, B.; Wu, A.G. Pose Measurement and Motion Estimation of Space Non-Cooperative Targets Based on Laser Radar and Stereo-vision Fusion. *IEEE Sens. J.* **2018**, *19*, 3008–3019. [CrossRef]
72. Lestarquit, L.; Harr, J.; Grelier, T.; Peragin, E.; Wilhelm, N.; Mehlen, C.; Peyrotte, C. Autonomous Formation Flying RF Sensor Development for the PRISMA Mission. In Proceedings of the 19th International Technical Meeting of the Satellite Division of the Institute of Navigation (ion Gnss 2006), Fort Worth, TX, USA, 26–29 September 2006.
73. Guo, C.; Xia, X.; Si, C.; Liu, P.; Yang, D. A Survey of Relative Position and Attitude Measurement for Formation Flying Satellite. *Aerosp. Control* **2018**, *36*, 83–89.
74. Liu, Y.; Dong-Yun, Y.I.; Wang, Z.M. Research on High Precision Measure Methods of Inter-Satellite Baselines of Formation Flying Satellites. *J. Astronaut.* **2007**, *6*, 1643–1647.
75. Opromolla, R.; Fasano, G.; Rufino, G.; Grassi, M. A Review of Cooperative and Uncooperative Spacecraft Pose Determination Techniques for Close-Proximity Operations. *Prog. Aeosp. Sci.* **2017**, *93*, 53–72. [CrossRef]
76. Wu, Y.; Cao, X.; Dan, X. Autonomous Relative Navigation for Formation Flying Satellites. In Proceedings of the International Symposium on Systems & Control in Aerospace & Astronautics, Harbin, China, 19–21 January 2006.
77. Schilling, K. Small Satellite Formations: Challenges in Navigation and its Application Potential. In Proceedings of the 2021 28th Saint Petersburg International Conference on Integrated Navigation Systems (ICINS), Saint Petersburg, Russia, 31 May–2 June 2021; pp. 1–4.
78. Bucolo, M.; Buscarino, A.; Famoso, C.; Fortuna, L.; Gagliano, S. Imperfections in Integrated Devices Allow the Emergence of Unexpected Strange Attractors in Electronic Circuits. *IEEE Access* **2021**, *9*, 29573–29583. [CrossRef]
79. Hou, R.; Zhao, S.H.; Jie, X.U.; Yong-Jun, L.I.; Ji-Li, W.U. The Effects Analysis of High Particles on the Laser Satellite Communication System. *Opt. Commun. Technol.* **2008**, *9*, 55–58.
80. Maessen, D.C.; Gill, E. Relative State Estimation and Observability for Formation Flying Satellites in the Presence of Sensor Noise. *Acta Astronaut.* **2013**, *82*, 129–136. [CrossRef]
81. Boscherini, M.; Adriani, O.; Bongi, M.; Bonechi, L.; Castellini, G.; D'Alessandro, R.; Gabbanini, A.; Grandi, M.; Menn, W.; Papini, P.; et al. Radiation Damage of Electronic Components in space Environment. *Nucl. Instrum. Methods Phys. Res. Sect. A-Accel. Spectrom. Dect. Assoc. Equip.* **2003**, *514*, 112–116. [CrossRef]
82. Godard; Kumar, K.D. Fault Tolerant Reconfigurable Satellite Formations Using Adaptive Variable Structure Techniques. *J. Guid. Control Dyn.* **2010**, *33*, 969–984. [CrossRef]
83. Salvoldi, M.; Choukroun, D. Intersatellite Laser Ranging and Attitude Robust Measurement Planning. In Proceedings of the Israel Conference on Aerospace Sciences, San Diego, CA, USA, 4–8 January 2016.
84. Li, J.; Kumar, K.D. Fault Tolerant Attitude Synchronization Control during Formation Flying. *J. Aerosp. Eng.* **2011**, *24*, 251–263. [CrossRef]
85. Sabatini, M.; Reali, F.; Palmerini, G.B. Autonomous State Estimation in Formation Flight. In Proceedings of the 2007 Ieee Aerospace Conference, Big Sky, MT, USA, 3–10 March 2007; IEEE: New York, NY, USA, 2007; Volumes 1–9, p. 628.
86. Balesdent, M.; Bérend, N.; Dépincé, P. New Multidisciplinary Design Optimization Approaches for Launch Vehicle Design. *Proc. Inst. Mech. Eng. Part G J. Aerosp. Eng.* **2012**, *227*, 1545–1555. [CrossRef]
87. Ujiie, R.; Nishi, K. Multi-Disciplinary System Design Optimization for All-Electric Geostationary Communication Satellite. In Proceedings of the 2018 IEEE Aerospace Conference, Big Sky, MT, USA, 3–10 March 2018; pp. 1–9.
88. Sobieszczanski-Sobieski, J. Multidisciplinary Design Optimization: An Emerging New Engineering Discipline. In *Advances in Structural Optimization*; NASA Langley Research Center: Hampton, VA, USA, 1993.
89. Balesdent, M.; Price, N.; Riche, R.L.; Kim, N.H.; Haftka, R.T. Advanced Space Vehicle Design Taking into Account Multidisciplinary Couplings and Mixed Epistemic/Aleatory Uncertainties. In *Space Engineering*; Springer International Publishing: Cham, Switzerland, 2016; Volume 114, pp. 1–48. [CrossRef]
90. Budianto, I.A.; Olds, J.R. A Collaborative Optimization Approach to Design and Deployment of a Space Based Infrared System Constellation. In Proceedings of the Aerospace Conference, Big Sky, MT, USA, 25–25 March 2000.
91. Curry, M.; Tour, P.L.; Slagowski, S. Multidisciplinary Design Optimization for a High-Resolution Earth-Imaging Constellation. In Proceedings of the 2015 IEEE Aerospace Conference, Big Sky, MT, USA, 7–14 March 2015. [CrossRef]

92. Roberto, D.P.; Alfredo, R. A Robust Crater Matching Algorithm for Autonomous Vision-Based Spacecraft Navigation. In Proceedings of the 2021 IEEE 8th International Workshop on Metrology for AeroSpace (MetroAeroSpace), Naples, Italy, 23–25 June 2021; pp. 322–327.
93. Zhang, C.; Liu, H.; Liu, Y. Combining Stereo Vision and Inertial Navigation for Inspection Spacecraft. In Proceedings of the 2019 Chinese Automation Congress (CAC), Hangzhou, China, 22–24 November 2019; pp. 2369–2374.
94. Rodrigues Ferreira, P.V.; Paffenroth, R.; Wyglinski, A.M.; Hackett, T.M.; Bilen, S.G.; Reinhart, R.C.; Mortensen, D.J. Multiobjective Reinforcement Learning for Cognitive Satellite Communications Using Deep Neural Network Ensembles. *IEEE J. Sel. Areas Commun.* **2018**, *36*, 1030–1041. [CrossRef]
95. Cheng, Y.-H.; Jiang, B.; Li, H.; Han, X. On-orbit Reconfiguration Using Adaptive Dynamic Programming for Multi-Mission-Constrained Spacecraft Attitude Control System. *Int. J. Control Autom. Syst.* **2019**, *17*, 822–835. [CrossRef]
96. Davis, J.C.; Pernicka, H. Spacecraft Identification Leveraging Unsupervised Learning Techniques for Formation and Swarm Missions. In Proceedings of the AIAA Scitech 2020 Forum, Orlando, FL, USA, 6–10 January 2020.
97. Long, J.; Qian, Z.; Xie, F.; Ding, Z.; Liu, L. An Improved Multi-Satellite Cooperative Task Planning Method Based on Distributed Multi-Agent System. In Proceedings of the 2021 13th International Conference on Measuring Technology and Mechatronics Automation (ICMTMA), Beihai, China, 16–17 January 2021; pp. 539–542.
98. Hu, X.; Liao, X.; Liu, Z.; Liu, S.; Ding, X.; Helaoui, M.; Wang, W.; Ghannouchi, F.M. Multi-Agent Deep Reinforcement Learning-Based Flexible Satellite Payload for Mobile Terminals. *IEEE Trans. Veh. Technol.* **2020**, *69*, 9849–9865. [CrossRef]
99. Hou, R.; Zhao, S.; Xu, J.; Wu, J.; Li, Y.; Zhan, S.; Shi, L.; Fang, S. Influence of Space Charged Particles on Satellite Optical Communication System. *Opt. Appl.* **2009**, *39*, 251–265.
100. Patraev, V.E.; Shangina, E.A.; Dvirny, V.V.; Voroshilova, A.A.; Borisov, S.A. Ensuring the Quality of the Materials Used in the Spacecraft Engineering. In Proceedings of the IX International Multidisciplinary Scientific and Research Conference Modern Issues in Science and Technology/Workshop Advanced Technologies in Aerospace, Mechanical and Automation Engineering, Nanjing, China, 17–19 August 2018; Iop Publishing Ltd.: Bristol, UK, 2018; Volume 450, p. 022010.
101. Wu, G.; Wang, L.; Ling, F. Research on Software Defined Payload Reconstruction Technology Scheme. In *China Satellite Navigation Conference (CSNC) 2020 Proceedings: Volume II*; Sun, J., Yang, C., Xie, J., Eds.; Lecture Notes in Electrical Engineering; Springer: Singapore, 2020; Volume 651, pp. 663–672. ISBN 9789811537103.
102. Maheshwarappa, M.R.; Bridges, C.P. Software Defined Radios for Small Satellites. In Proceedings of the 2014 Nasa/Esa Conference on Adaptive Hardware and Systems (ahs), Leicester, UK, 14–17 July 2014; IEEE: New York, NY, USA, 2014; pp. 172–179.
103. Wang, J.; Zhang, R.; Yuan, J. Luo Multi-CubeSat Relative Position and Attitude Determination Based on Array Signal Detection in Formation Flying. *IEEE Trans. Aerosp. Electron. Syst.* **2019**, *55*, 3378–3393. [CrossRef]